This article has not been copyedited and formatted. The final version may differ from this version.
Molecular Pharmacology Fast Forward. Published on October 1, 2013 as doi:10.1124/mol.113.088393

Cellular Uptake of the Anti-Tumor Agent, Dp44mT, Occurs *via* a Carrier/Receptor-Mediated Mechanism.

Angelica M. Merlot, Namfon Pantarat, Sharleen V. Menezes, Sumit Sahni, Des R. Richardson and Danuta S. Kalinowski

Molecular Pharmacology and Pathology Program, Department of Pathology and Bosch Institute, University of Sydney, Sydney, NSW 2006 Australia.

Molecular Pharmacology Fast Forward. Published on October 1, 2013 as DOI: 10.1124/mol.113.088393
This article has not been copyedited and formatted. The final version may differ from this version.

Running title: Carrier/receptor-mediated uptake of Dp44mT.

Authors for Correspondence: Dr. Danuta Kalinowski and Dr. Des Richardson, Molecular Pharmacology and Pathology Program, Department of Pathology and Bosch Institute, University of Sydney, Sydney, NSW 2006 Australia. Ph: + 61-2-9036-6547; FAX: +61-2-9351-3429; Email: danuta.kalinowski@sydney.edu.au; d.richardson@med.usyd.edu.au.

Text Pages: 37

Tables: 1 plus 1 Supplementary Table.

Figures: 9 plus 4 Supplementary Figures.

References: 60

Word Count: - Abstract: 250
- Introduction: 702
- Discussion: 1474

Abbreviations: 44mT, 4,4-dimethyl-3-thiosemicarbazide; Ap4eT, 2-acetylpyridine 4-ethyl-3-thiosemicarbazone; Ap4mT, 2-acetylpyridine 4-methyl-3-thiosemicarbazone; Ap44mT, 2-acetylpyridine 4,4-dimethyl-3-thiosemicarbazone; Ap4pT, 2-acetylpyridine 4-phenyl-3-thiosemicarbazone; ApT, 2-acetylpyridine thiosemicarbazone; B_{max}, maximum number of binding sites; Bp4aT, 2-benzoylpyridine 4-allyl-3-thiosemicarbazone; Bp4eT, 2-benzoylpyridine 4-ethyl-3-thiosemicarbazone; Bp4mT, 2-benzoylpyridine 4-methyl-3-thiosemicarbazone; Bp44mT, 2-benzoylpyridine 4,4-dimethyl-3-thiosemicarbazone; BpT, 2-benzoylpyridine thiosemicarbazone; DFO, desferrioxamine; Dp4aT, di-2-pyridylketone 4-allyl-3-thiosemicarbazone; Dp4eT, di-2-pyridylketone 4-ethyl-3-thiosemicarbazone; Dp4mT, di-2-pyridylketone 4-methyl-3-thiosemicarbazone; Dp44mT, di-2-pyridylketone 4,4-dimethyl-3-thiosemicarbazone; Dp4pT, di-2-pyridylketone 4-phenyl-3-thiosemicarbazone; DpC, di-2-pyridylketone 4-cyclohexyl-4-methyl-3-thiosemicarbazone; DpK, di-2-pyridylketone; DpT, di-2-pyridylketone thiosemicarbazone; K_d, equilibrium dissociation constant; PIH, pyridoxal isonicotinoyl hydrazone; RR, ribonucleotide reductase; Tf, transferrin; TfR1, transferrin receptor 1.

Molecular Pharmacology Fast Forward. Published on October 1, 2013 as DOI: 10.1124/mol.113.088393
This article has not been copyedited and formatted. The final version may differ from this version.

Abstract

The chelator, di-2-pyridylketone 4,4-dimethyl-3-thiosemicarbazone (Dp44mT), shows potent and selective anti-cancer and anti-metastatic activity. However, the mechanism by which it is initially transported into cells to induce cytotoxicity is unknown. Hence, the current investigation examined the cellular uptake of ^{14}C-Dp44mT relative to two structurally-related ligands, namely the aroylhydrazone, ^{14}C-pyridoxal isonicotinoyl hydrazone (^{14}C-PIH), and the thiosemicarbazone, ^{14}C-2-benzoylpyridine 4-ethyl-3-thiosemicarbazone (^{14}C-Bp4eT). In marked contrast to the cellular uptake of ^{14}C-PIH and ^{14}C-Bp4eT that were linear as a function of concentration, ^{14}C-Dp44mT uptake was saturable using SK-N-MC neuroepithelioma cells (B_{max} 4.28 x 10^7 molecules of chelator/cell and K_d 2.45 μM). Together with the fact that ^{14}C-Dp44mT uptake was temperature-dependent and significantly ($p < 0.01$) decreased by competing unlabeled Dp44mT, these observations indicated a saturable transport mechanism consistent with carrier/receptor-mediated transport. Other unlabeled ligands that shared the saturated N4 structural moiety with Dp44mT significantly ($p < 0.01$) inhibited ^{14}C-Dp44mT uptake, illustrating its importance for carrier/receptor recognition. Nevertheless, unlabeled Dp44mT most markedly decreased ^{14}C-Dp44mT uptake, demonstrating that the putative carrier/receptor shows high selectivity for Dp44mT. Interestingly, in contrast to ^{14}C-Dp44mT, uptake of its Fe complex [Fe(^{14}C-Dp44mT)$_2$] was not saturable as a function of concentration and was much greater than the ligand alone, indicating an alternate mode of transport. Studies examining the tissue distribution of ^{14}C-Dp44mT injected intravenously into a mouse tumor model demonstrated the ^{14}C label was primarily identified in the excretory system. Collectively, these findings examining the mechanism of Dp44mT uptake and its distribution and excretion have clinical implications for its bioavailability and uptake *in vivo*.

Molecular Pharmacology Fast Forward. Published on October 1, 2013 as DOI: 10.1124/mol.113.088393
This article has not been copyedited and formatted. The final version may differ from this version.

Introduction

Intensive research has established that cancer cells have distinctly altered signaling pathways, enabling uncontrolled proliferation (Hanahan and Weinberg, 2011). Interestingly, emerging evidence demonstrates that iron (Fe) homeostasis is perturbed in cancer cells (Merlot et al., 2013). For instance, compared to normal cells, tumor cells have higher levels of the transferrin receptor 1 (TfR1), that is responsible for Fe uptake from the Fe transport protein, transferrin (Tf) (Soyer et al., 1987). This increased TfR1 expression also correlates with tumor grade and stage (Seymour et al., 1987; Soyer et al., 1987). Additionally, the Fe-dependent enzyme, ribonucleotide reductase (RR), which catalyzes the rate-limiting step in DNA synthesis, is up-regulated in cancer cells (Elford et al., 1970; Takeda and Weber, 1981). Changes in Fe trafficking proteins have also been observed in cancer cells, including ferritin and ferroportin 1 (Merlot et al., 2013; Pinnix et al., 2010). Together, these alterations in Fe metabolism impart neoplastic cells with a “high intracellular Fe” phenotype (Pinnix et al., 2010).

Due to their high metabolic requirement for Fe, malignant cells are sensitive to iron deprivation using chelators (Buss et al., 2003; Kalinowski and Richardson, 2005). One of the most potent groups of chelators with anti-cancer activity include the di-2-pyridylketone thiosemicarbazone (DpT) series, in particular di-2-pyridylketone 4,4-dimethyl-3-thiosemicarbazone (Dp44mT, Fig. 1; Whitnall et al., 2006; Yuan et al., 2004). The broad and potent anti-cancer activity of Dp44mT has been shown in >30 tumor cell-types, including drug-resistant and p53 mutant cells (Rao et al., 2009; Tian et al., 2010; Whitnall et al., 2006).

In terms of its effects *in vivo*, Dp44mT inhibited tumor growth in multiple tumor mouse models, including human pancreatic, melanoma, and neuroepithelioma xenografts (Kovacevic et al., 2011; Whitnall et al., 2006), as well as reducing metastasis in a breast cancer model

Molecular Pharmacology Fast Forward. Published on October 1, 2013 as DOI: 10.1124/mol.113.088393
This article has not been copyedited and formatted. The final version may differ from this version.

(Liu et al., 2012). Relative to the thiosemicarbazone, Triapine® (Fig. 1), that has been examined in >20 Phase I and II international clinical trials (Merlot et al., 2013), a 30-fold lower dose of Dp44mT was necessary to induce the same anti-tumor activity *in vivo* (Whitnall et al., 2006).

Interestingly, Dp44mT has a variety of molecular targets. The ligand can potently mobilize intracellular Fe and also prevent cellular Fe uptake from Tf (Yuan et al., 2004). Furthermore, Dp44mT increases the expression of the potent metastasis suppressor, *N-myc downstream regulated gene 1* (Kovacevic et al., 2011; Le and Richardson, 2004). Due to its ability to deplete cellular Fe (Yuan et al., 2004), Dp44mT causes cell cycle arrest at the G_1/S phase (Noulsri et al., 2009; Rao et al., 2009) and inhibits the activity of the Fe-dependent enzyme, RR, impeding cellular DNA synthesis and proliferation (Yu et al., 2011). Interestingly, Dp44mT was observed to accumulate within lysosomes where it forms redox-active copper (Cu) complexes that induce oxidative damage and lysosomal permeabilization (Lovejoy et al., 2011). This latter event results in the release of cathepsins that lead to the cleavage of pro-apoptotic Bid and apoptosis (Lovejoy et al., 2011).

While much has been revealed concerning the intracellular targets of Dp44mT, understanding the mechanisms involved in the membrane transport of the drug remain undeciphered and is the subject of this investigation. In fact, little is known regarding the membrane transport mechanisms of iron chelators in mammalian cells. It has been demonstrated that ligand lipophilicity plays a critical role in their uptake and activity (Baker et al., 1985; Porter et al., 1988). Hydrophilic ligands such as desferrioxamine (DFO) show slow uptake relative to more lipophilic chelators (Richardson et al., 1994). Indeed, a direct correlation is found between increased lipophilicity and greater iron chelation efficacy and anti-proliferative activity (Richardson et al., 1995). A previous study demonstrated that the cellular uptake of

thiosemicarbazone, 2-benzoylpyridine 4-ethyl-3-thiosemicarbazone (Bp4eT; Fig. 1), occurred *via* an energy-independent and temperature-independent uptake mechanism consistent with passive diffusion (Merlot et al., 2010).

In this investigation, Dp44mT was labeled with ^{14}C to assess membrane transport in tumor cells. These studies were performed in comparison to several chelators that show structural similarity, namely Bp4eT and the aroylhydrazone, pyridoxal isonicotinoyl hydrazone (PIH; Fig. 1), whose uptake mechanisms were previously characterized and act as internal controls (Merlot et al., 2010). Our results demonstrate that in contrast to Bp4eT and PIH, Dp44mT is transported into cells by a saturable carrier/receptor-mediated mechanism.

Molecular Pharmacology Fast Forward. Published on October 1, 2013 as DOI: 10.1124/mol.113.088393
This article has not been copyedited and formatted. The final version may differ from this version.

Materials and Methods

Chelators and Other Reagents

The ^{14}C-Bp4eT, ^{14}C-PIH and ^{14}C-Dp44mT was synthesized and characterized by the Institute of Isotopes Ltd (Budapest, Hungary) with the isotope, ^{14}C, incorporated at the imine carbon (see asterisk, Fig. 1). The certificate of analysis of the labeled ^{14}C-chelators indicated the compounds were 98.5-100% pure and had a final specific activity of 75 μCi/mg. The Fe(III) and Cu(II) ^{14}C-complexes were prepared by adding ferric chloride ($FeCl_3$; Sigma-Aldrich, St. Louis, MO, USA) or cupric sulfate ($CuSO_4$; Sigma-Aldrich), respectively, at a 2:1 (^{14}C-chelator:metal) molar ratio. Human Tf was purchased from Sigma-Aldrich. The following radionuclides were purchased from PerkinElmer (Waltham, MA): $^{59}FeCl_3$ dissolved in 0.5 M HCl (Cat. # NEZ037) and "carrier-free" $Na^{125}I$ dissolved in 10 mM NaOH (specific activity = 17.4 mCi/mg; Cat. # NEZ033A).

In competition experiments with the ^{14}C-labeled ligands above, non-labeled chelators or their precursors were utilized (for protocol see *"^{14}C-Chelator Cellular Uptake"* below). The synthesis and characterization of these compounds have been described in detail in previous publications (Jansson et al., 2010; Kalinowski et al., 2007; Richardson et al., 2006; Yuan et al., 2004) and include: **(1)** chelators of the DpT series (namely: di-2-pyridylketone thiosemicarbazone, DpT; di-2-pyridylketone 4-methyl-3-thiosemicarbazone, Dp4mT; di-2-pyridylketone 4,4-dimethyl-3-thiosemicarbazone, Dp44mT; di-2-pyridylketone 4-ethyl-3-thiosemicarbazone, Dp4eT; di-2-pyridylketone 4-allyl-3-thiosemicarbazone, Dp4aT; di-2-pyridylketone 4-phenyl-3-thiosemicarbazone, Dp4pT; and di-2-pyridylketone 4-cyclohexyl-4-methyl-3-thiosemicarbazone, DpC; Supplementary Fig. 1A); **(2)** Dp44mT precursors (namely: di-2-pyridylketone, DpK, and 4,4-dimethyl-3-thiosemicarbazide, 44mT; Supplementary Fig. 1A); **(3)** the 2-benzoylpyridine thiosemicarbazone (BpT) series (namely:

Molecular Pharmacology Fast Forward. Published on October 1, 2013 as DOI: 10.1124/mol.113.088393
This article has not been copyedited and formatted. The final version may differ from this version.

2-benzoylpyridine thiosemicarbazone, BpT; 2-benzoylpyridine 4-methyl-3-thiosemicarbazone, Bp4mT; 2-benzoylpyridine 4,4-dimethyl-3-thiosemicarbazone, Bp44mT; 2-benzoylpyridine 4-ethyl-3-thiosemicarbazone, Bp4eT; and 2-benzoylpyridine 4-allyl-3-thiosemicarbazone, Bp4aT; Supplementary Fig. 1B); and **(4)** the 2-acetylpyridine thiosemicarbazone (ApT) series (namely: 2-acetylpyridine thiosemicarbazone, ApT; 2-acetylpyridine 4-methyl-3-thiosemicarbazone, Ap4mT; 2-acetylpyridine 4,4-dimethyl-3-thiosemicarbazone, Ap44mT; 2-acetylpyridine 4-ethyl-3-thiosemicarbazone, Ap4eT; and 2-acetylpyridine 4-phenyl-3-thiosemicarbazone, Ap4pT; Supplementary Fig. 1C). Chelators were dissolved in DMSO (Sigma-Aldrich) and diluted in complete medium so that the final DMSO concentration was < 0.5% (v/v).

Cell Culture

The human SK-N-MC neuroepithelioma, DMS-53 lung carcinoma, SK-Mel-28 melanoma and MRC-5 fibroblast cell lines were obtained from the American Type Culture Collection (ATCC; Manassas, VA). The SK-N-MC, SK-Mel-28 and MRC-5 cell-types were cultured in Minimal Essential Medium (MEM; Life Technologies, Mulgrave, Victoria, Australia), while the DMS-53 cell type was grown in Roswell Park Memorial Institute 1640 (RPMI 1640; Life Technologies). These media were supplemented with 10% (v/v) fetal calf serum (FCS; Sigma-Aldrich) and the following additives from Life Technologies: 1% (v/v) sodium pyruvate, 1% (v/v) non-essential amino acids, 100 U/mL penicillin, 100 µg/mL streptomycin, 2 mM glutamine and 0.28 ng/mL Fungizone. The cells were then incubated at 37^{o}C in 5% CO_2 and 95% atmosphere, as previously described (Merlot et al., 2010).

Preparation of ^{59}Fe-^{125}I-Transferrin

Human apo-Tf (Sigma-Aldrich) was labeled with ^{59}Fe to produce the ^{59}Fe trace-labeled di-ferric protein,$^{59}Fe_2$-Tf using standard procedures (Richardson and Baker, 1990). The $^{59}Fe_2$-Tf

Molecular Pharmacology Fast Forward. Published on October 1, 2013 as DOI: 10.1124/mol.113.088393
This article has not been copyedited and formatted. The final version may differ from this version.

was further labeled with ^{125}I (supplied as carrier-free $Na^{125}I$; Perkin-Elmer) using an adaptation of the iodine monochloride method of Mc Farlane (Mc Farlane, 1958) to produce doubly-labeled $^{59}Fe_2$-^{125}I-Tf (Richardson and Baker, 1990). Unbound ^{59}Fe and ^{125}I were thoroughly removed by exhaustive vacuum dialysis (Richardson and Baker, 1990).

^{14}C-Chelator Cellular Uptake

Uptake of the ^{14}C-chelator by cells was performed as described previously (Merlot et al., 2010) for up to 120 min at 4^{o}C or 37^{o}C in medium that, unless specified otherwise, contained the ^{14}C-chelator (25 μM), 10% FCS and all of the supplements described above. Notably, the medium used throughout our investigation contains only trace levels of Fe *i.e.*, <1.8 μM (personal communication, Technical Support, Life Technologies). Moreover, as already stated, our studies implement this media supplemented with 10% FCS which contains the avid iron-binding protein, Tf, at a final concentration of 2 μM (personal communication, Technical Support, Life Technologies). This means that any low molecular weight iron will be effectively bound to Tf which has an extremely high Fe-binding affinity (K_a*:* 10^{24} M^{-1}; (Chung, 1984)). Similarly, it is also known that Tf binds copper ion with appreciable avidity (Chung, 1984), and would also lead to media that is depleted of this metal ion. Since we are generally using ligands at a concentration of 25 μM, the formation of Fe or Cu complexes by the ^{14}C-chelators in the medium prior to cellular uptake would be insignificant. Similarly, in the serum of mammals, almost all the iron and copper is bound to Tf and ceruloplasmin, respectively (Chung, 1984; Hsieh and Frieden, 1975), and is not in a low molecular weight form which can be easily chelated by these types of aroylhydrazone and thiosemicarbazone ligands (Richardson et al., 2009).

In competition experiments, unlabeled agents were incubated with cells for 120 min at 37^{o}C at concentrations of 2.5, 5, 25, 50, 100, 150 or 250 μM in the presence of labeled ^{14}C-chelator

Molecular Pharmacology Fast Forward. Published on October 1, 2013 as DOI: 10.1124/mol.113.088393
This article has not been copyedited and formatted. The final version may differ from this version.

(25 μM). The unlabeled chelators and precursors utilized included those described above in "*Chelators and Other Reagents*" (Supplementary Fig. 1), as well as Triapine® and PIH (Fig. 1). At each time point, uptake was inhibited by chilling cells in Petri dishes to 4°C on a tray of ice and washing the monolayer four times with ice-cold PBS, as per standard labeling protocols (Merlot et al., 2010). Cells were then removed from the plates using a teflon spatula in 1 mL of PBS and added to scintillation vials. Scintillation fluid (2.5 mL; PerkinElmer Life and Analytical Sciences, VIC, Australia) was added to these cell suspensions and the radioactivity measured using a Wallac 1450 MicroBeta TriLux Counter (Perkin Elmer Life and Analytical Sciences) with appropriate calibration standards and backgrounds. Results were expressed as molecules of chelator/cell or as uptake (% control). Non-linear regression analysis was performed on data obtained from studies examining cellular uptake as a function of concentration. Binding curves were analyzed using GraphPad Prism 5.0 (GraphPad Software, San Diego, CA) to determine the maximum number of binding sites (B_{max}) and the equilibrium dissociation constant (K_d).

Effect of Metabolic Inhibitors on ^{14}C-Dp44mT Uptake

The effect of two well characterized metabolic inhibitors (Sigma-Aldrich), namely: sodium azide (NaN_3; 30 mM) and sodium cyanide (NaCN; 5 mM) were assessed on the uptake of ^{14}C-Dp44mT by cells. In brief, SK-N-MC neuroepithelioma cells were preincubated with inhibitors or media alone for 30 min/37°C. The media were then removed and replaced with media containing ^{14}C-Dp44mT (25 μM) or ^{59}Fe-^{125}I-transferrin (0.75 μM) in the presence or absence of inhibitors, and incubated for 60 min/37°C. The remainder of the experiment was conducted using the general uptake procedure above. During these studies, Dulbecco's modified Eagle's medium without glucose (DMEM - GLU; Invitrogen) was used to aid the ATP-depletion induced by the metabolic inhibitors (Merlot et al., 2010; Richardson, 1997). As a positive control for ATP depletion and inhibition of receptor-mediated endocytosis, ATP

Molecular Pharmacology Fast Forward. Published on October 1, 2013 as DOI: 10.1124/mol.113.088393
This article has not been copyedited and formatted. The final version may differ from this version.

levels and the uptake of ^{59}Fe-^{125}I-transferrin were examined concurrently under these incubation conditions as they are well known to be markedly reduced by these inhibitors (Iacopetta and Morgan, 1983; Merlot et al., 2010; Morgan and Baker, 1969). ATP levels were quantitatively analysed using an ATP bioluminescence assay kit (Sigma-Aldrich) following the manufacturer's instructions, as described previously (Merlot et al., 2010). Results were expressed as a percentage of the control.

^{14}C-Chelator Cellular Efflux

SK-N-MC cells were pre-labeled with ^{14}C-chelator (25 μM) for 120 min/37^{o}C following standard methods (Merlot et al., 2010). Then, this labeling medium was removed by aspiration and the cells in Petri dishes were chilled to 4^{o}C on a tray of ice and washed four times with ice-cold PBS. Fresh medium was subsequently added to the dishes and the cells re-incubated at an appropriate temperature (4^{o}C or 37^{o}C) over various time points for up to 180 min. The medium overlying the cells was then collected and placed into scintillation vials and the cells removed from the Petri dishes in 1 mL of PBS using a Teflon spatula and placed into separate vials. Samples (medium and cells) were then analyzed for radioactivity using the β-counter above to determine the percentage of cellular radiolabel released into the medium.

Tumor Xenograft Model in Nude Mice

Six week old, female BALB/c nu/nu mice were obtained from the Animal Resources Centre (Canning Vale, Perth, WA) and used for studies after acclimatization within the facility at 7 weeks of age. The mice were housed in sterile conditions in the University of Sydney, Bosch Animal House where they received food and water *ad libitum*. All *in vivo* experiments were approved by the Animal Ethics Committee (University of Sydney). To generate tumor xenografts, DMS-53 lung carcinoma cells were harvested and suspended in RPMI media devoid of added supplements. The viable cell number was determined by Trypan-blue dye

Molecular Pharmacology Fast Forward. Published on October 1, 2013 as DOI: 10.1124/mol.113.088393
This article has not been copyedited and formatted. The final version may differ from this version.

exclusion using a Countess™ Automated Cell Counter (Life Technologies, Carlsbad, CA, USA) and was always > 95%. A final density of 10^8 cells/mL was obtained and mixed with an equal volume of cold Matrigel (BD Biosciences, San Jose, CA). Matrigel was kept on ice at 4^oC to prevent polymerization and solidification.

Prior to implantation, mice were anaesthetised with isoflurane (Sigma-Aldrich). DMS-53 cells (5×10^6 cells; 100 µL) were subcutaneously injected into the right hind flank of each mouse (Whitnall et al., 2006; Yu et al., 2012). Tumor growth was calculated in mm^3 by measuring the two perpendicular diameters of the tumors with Vernier calipers. Tumor volume was estimated using the formula ($L/2 \times W^2$), where L was the longest diameter (length) and W was the shortest diameter (width) perpendicular to L (Balsari et al., 2004). Measurements and mouse body weight changes were made and recorded twice weekly.

A single dose of radiolabeled chelator was initiated 3 weeks after implantation, once the mean tumor volume reached ~400 mm^3. Experimental groups were randomized and each group (n = 16) received either ^{14}C-Bp4eT, ^{14}C-PIH or ^{14}C-Dp44mT supplemented with unlabeled Bp4eT, PIH or Dp44mT, respectively, to yield a final dose of 2 mg/kg of body weight, and a final specific activity of 1 µCi (chelator specific radioactivity: 75 µCi/mg). Chelators were dissolved in a vehicle consisting of 30% sterile propylene glycol (Sigma-Aldrich) and 70% sterile saline (0.9% NaCl; Baxter, Old Toongabbie, NSW, Australia) and administered intravenously *via* the tail vein (100 µL/mouse). Chelator-treated groups (n =16) were further subdivided into four groups (n = 4) according to the following time points: 0.5, 1, 4 and 24 h. Control mice (n = 4) were treated with vehicle alone. Animals were placed in metabolic cages during these studies in groups of 4 in order to collect urine and feces.

At 0.5, 1, 4 and 24 h post-administration, mice were anaesthetized with isoflurane and blood

Molecular Pharmacology Fast Forward. Published on October 1, 2013 as DOI: 10.1124/mol.113.088393
This article has not been copyedited and formatted. The final version may differ from this version.

samples were collected by cardiac puncture. To eliminate residual radioactivity of blood in tissues, mice underwent intra-cardiac perfusion with 10 mL of PBS injected into the left ventricle with the right atrium being incised to allow release of blood. Following perfusion, mice were euthanized by cervical dislocation and were immediately dissected. The liver, gallbladder, kidneys, lungs, spleen, brain, bladder, large intestine, small intestine, bone (left femur), skeletal muscle (left thigh) and peri-renal adipose tissue were removed and weighed. Femurs were cleaned of connective tissue and muscle. Feces and urine were collected from metabolic cages for each group (n = 4) during the specified time points.

Sample Combustion

Tissue, blood, fecal and urine samples, from *in vivo* administration experiments with ^{14}C-labeled ligands, were combusted using a Sample Oxidizer Model 307 (Perkin Elmer Life and Analytical Sciences). Combustion of the tissues *etc* was essential to prevent radioactive quenching and the inaccurate quantification of ^{14}C (Moore, 1981). Wet weights of tissue and whole organs were recorded prior to combustion and large tissues or organs (> 400 mg) were homogenized and a 300 mg aliquot was combusted due to the sample weight limitations of the machine. Blood samples were placed in a heparinized tube and centrifuged to allow the sedimentation of blood cells from plasma. A 10 µL aliquot of urine and a 100 µL aliquot of blood and serum were combusted. Samples were placed within combustion cones with the combustion process aided using 250 µL of Combustaid (Perkin Elmer Life and Analytical Sciences) per sample with combustion being performed for 2 min. After combustion, $^{14}CO_2$ was trapped by 10 mL of Carbo-Sorb® E (Perkin Elmer Life and Analytical Sciences) and mixed with 10 mL of Permafluor® E^+ scintillant (Perkin Elmer Life and Analytical Sciences). The combustion efficiency of the oxidizer was determined using ^{14}C standards before each run of the instrument and was always >97%.

Molecular Pharmacology Fast Forward. Published on October 1, 2013 as DOI: 10.1124/mol.113.088393
This article has not been copyedited and formatted. The final version may differ from this version.

Radioactive samples from the combustion process were analyzed using the β-counter described above. Background radioactivity was measured using corresponding samples from control animals that were administered the vehicle alone. Results were expressed as % of injected dose (ID)/g of organs, tissues and feces or % of ID/μL of urine.

Statistical Analysis

Results are expressed as mean ± standard error of the mean (S.E.M.). Statistical comparisons were made using the Student's *t*-test and were considered statistically significant when $p < 0.05$.

Molecular Pharmacology Fast Forward. Published on October 1, 2013 as DOI: 10.1124/mol.113.088393
This article has not been copyedited and formatted. The final version may differ from this version.

Results

^{14}C-Dp44mT Uptake as a Function of Concentration is Saturable and Temperature Dependent

The cellular uptake of ^{14}C-Dp44mT, ^{14}C-Bp4eT or ^{14}C-PIH by SK-N-MC neuroepithelioma cells was examined over a range of concentrations for 2 h at 4^{o}C and 37^{o}C (Fig. 2). This cell-type was initially used as its response to these chelators has been well characterized in our laboratory (Kalinowski et al., 2007; Merlot et al., 2010; Richardson and Ponka, 1994; Richardson et al., 2006; Richardson et al., 1995). Notably, at 37^{o}C, cycling carriers or receptors (*i.e.*, internalized and membrane-bound) can be detected, while at 4^{o}C endocytosis and exocytosis are inhibited and only membrane-bound carriers/receptors are found (Harding et al., 1983; Morgan, 1981). Importantly, a 2 h incubation was utilized in these studies for four reasons: **(1)** to ensure that a steady state had been reached between ligand uptake and efflux, as judged from previous studies (Merlot et al., 2010; Yuan et al., 2004); **(2)** to prevent cytotoxicity of the ligands which was carefully assessed at the end of each incubation (using Trypan blue exclusion and cellular morphology); **(3)** to enable sufficient ^{14}C-ligand labeling of cells for sensitive detection; and **(4)** to prevent extensive metabolism of the ^{14}C-ligand that could potentially affect the results.

At 4^{o}C and 37^{o}C, ^{14}C-Dp44mT uptake increased as a function of concentration until it plateaued at 5 μM (Fig. 2A), which is consistent with a saturable transport mechanism. A non-linear regression fit for a one-binding site model reported a B_{max} value of 4.28 x 10^{7} ± 0.26 molecules of chelator/cell (n = 9) and a K_d value of 2.45 ± 0.67 μM (n = 9) at 37^{o}C (Table 1). This model was utilized as ligand uptake as a function of concentration was a single exponential curve. In contrast, at 4^{o}C, analysis of the data yielded a lower B_{max} value of 2.49 x 10^{7} ± 0.13 molecules of chelator/cell and a higher K_d value of 4.71 ± 1 μM.

Molecular Pharmacology Fast Forward. Published on October 1, 2013 as DOI: 10.1124/mol.113.088393
This article has not been copyedited and formatted. The final version may differ from this version.

Since ligand uptake at 37^{o}C represents total uptake (namely membrane and intracellular; (Harding et al., 1983)), while uptake at 4^{o}C represents membrane uptake only (Iacopetta and Morgan, 1983; Morgan, 1981), this enables calculation of the percentage of putative cycling carriers/receptors internalized. This analysis revealed that 62 ± 16% (Table 1) of binding sites were internalized, which is in general agreement with a variety of other cycling receptors *e.g.*, TfR1 (Ciechanover et al., 1983; Mulford and Lodish, 1988). Notably, similar saturable ^{14}C-Dp44mT uptake was also evident in other cell-types, including DMS-53 lung carcinoma and SK-Mel-28 melanoma cells, as well as mortal MRC-5 fibroblasts (Supplementary Fig. 2), suggesting expression of the carrier/receptor was widespread. The B_{max} and K_d values from the binding data in these latter cell-types (Supplementary Table 1) were generally similar to those obtained using SK-N-MC cells (Table 1). However, it is notable that the K_d from MRC-5 binding data was 2-5 fold higher than that found for the other 3 cell-types.

As demonstrated in our previous studies (Merlot et al., 2010) and in marked contrast to ^{14}C-Dp44mT, the uptake of ^{14}C-Bp4eT and ^{14}C-PIH increased linearly as a function of concentration in the range of 5-250 µM (Fig. 2B and C), without showing any evidence of saturation. Unlike ^{14}C-Dp44mT, the cellular uptake of ^{14}C-Bp4eT showed no significant (p > 0.05) difference at 4°C and 37°C (Fig. 2B). This observation suggested different mechanisms were involved in the uptake of these ligands. Additionally, ^{14}C-PIH uptake process was temperature-dependent (Fig. 2C), although, in contrast to ^{14}C-Dp44mT (Fig. 2A), no evidence of saturable binding was evident. In fact, incubating cells at 4^{o}C relative to 37^{o}C significantly (p < 0.05) decreased ^{14}C-PIH uptake by approximately 80%.

The Effect of Metabolic Inhibitors on ^{14}C-Dp44mT Uptake.

Considering the data above, studies were then performed to determine whether ^{14}C-Dp44mT

Molecular Pharmacology Fast Forward. Published on October 1, 2013 as DOI: 10.1124/mol.113.088393
This article has not been copyedited and formatted. The final version may differ from this version.

uptake was energy-dependent (Fig. 3A-D). The effect of two well characterized metabolic inhibitors, namely NaN_3 and NaCN (Henderson and Zevely, 1984; Qian and Morgan, 1991; Richardson, 1997), on ^{14}C-Dp44mT uptake into SK-N-MC cells was examined at 37°C (Fig. 3A). Importantly, NaN_3 (30 mM) and NaCN (5 mM) significantly (p<0.001) reduced ^{14}C-Dp44mT uptake to 56 ± 3 % and 68 ± 3% of the control, respectively. Concurrently, as positive controls, these inhibitors significantly (p < 0.01-0.001) decreased ATP levels as well as ^{59}Fe and ^{125}I-transferrin uptake (Fig. 3B-D), indicating these agents inhibited ATP synthesis and reduced receptor-mediated endocytosis, respectively, as shown previously (Merlot et al., 2010; Morgan and Baker, 1969). Together, with results showing the temperature-dependent uptake of ^{14}C-Dp44mT (Fig. 2A), these studies indicated an energy-dependent mechanism consistent with receptor-mediated endocytosis.

^{14}C-Dp44mT Uptake, But Not ^{14}C-Bp4eT or ^{14}C-PIH Uptake is Inhibited by its Unlabeled Ligand

Competitive binding between a ^{14}C-labeled ligand and the same non-labeled ligand should reduce uptake of the label if a saturable mechanism is involved. To examine this, the cellular uptake of ^{14}C-Dp44mT, ^{14}C-Bp4eT and ^{14}C-PIH at 37^{o}C was assessed in the presence of an increasing concentration of their corresponding unlabeled chelator (Fig. 4A-C). The uptake of ^{14}C-Dp44mT decreased with increasing concentrations of unlabeled Dp44mT (Fig. 4A), with this effect becoming significant (p < 0.001) at an unlabeled ligand concentration of 5 μM. This observation was consistent with competition with a saturable transport mechanism. Conversely, the uptake of ^{14}C-Bp4eT and ^{14}C-PIH was not significantly (p > 0.05) inhibited by their respective unlabeled drug (Fig. 4B and C). This observation is consistent with the uptake of ^{14}C-Bp4eT and ^{14}C-PIH by a non-carrier-mediated process.

Interestingly, ^{14}C-Bp4eT uptake was significantly (p < 0.001) increased in the presence of

Molecular Pharmacology Fast Forward. Published on October 1, 2013 as DOI: 10.1124/mol.113.088393
This article has not been copyedited and formatted. The final version may differ from this version.

high concentrations of unlabeled Bp4eT, namely at 100-250 μM (Fig. 4B). A similar, although not significant ($p > 0.05$), increase in ^{14}C-PIH uptake as a function of unlabelled ligand concentration was also observed (Fig. 4C). These data in Fig. 4B and 4C may be attributed to membrane perturbation by these agents which can increase binding of the radiolabel to cells (Baker et al., 1992).

^{14}C-Dp44mT Uptake is Not Affected by its Synthetic Precursors, DpK and 44mT

Considering the potential involvement of a carrier/receptor-mediated process in Dp44mT transport, the uptake of ^{14}C-Dp44mT (25 μM) was examined in the presence of increasing concentrations of its unlabeled precursors, namely DpK (2.5-250 μM) or 44mT (2.5-250 μM); Fig. 5A-C). These studies were performed in order to decipher the structural features necessary for the transport mechanism involved. As shown in Fig. 4A, ^{14}C-Dp44mT uptake was markedly decreased in the presence of unlabeled Dp44mT (Fig. 5A). In contrast, increasing concentrations of unlabeled DpK or 44mT had no significant effect ($p>0.05$) on ^{14}C-Dp44mT uptake in SK-N-MC cells (Fig. 5B and C). Therefore, neither of the direct precursors used to synthesize Dp44mT, namely, DpK nor 44mT, were able to compete for the putative carrier/receptor responsible for the uptake of Dp44mT by SK-N-MC cells.

Uptake of ^{14}C-Dp44mT is Only Inhibited by Ligands with Marked Structural Similarity

In view of the competitive uptake of ^{14}C-Dp44mT by its unlabeled counterpart (Fig. 4A), the effect of a range of structurally diverse thiosemicarbazone and aroylhydrazone ligands (100 μM) on ^{14}C-Dp44mT uptake (25 μM) was also assessed to determine carrier/receptor specificity (Fig. 6). Unlabeled ligands of the DpT series (DpT, Dp4mT, Dp44mT, Dp4eT, Dp4aT, Dp4pT and DpC), the BpT series (BpT, Bp4mT, Bp44mT, Bp4eT and Bp4aT) and the ApT series (ApT, Ap4mT, Ap44mT, Ap4eT and Ap4pT), as well as Triapine® and PIH, were assessed because of the various similarities and differences in their structure (Supplementary

Molecular Pharmacology Fast Forward. Published on October 1, 2013 as DOI: 10.1124/mol.113.088393
This article has not been copyedited and formatted. The final version may differ from this version.

Fig. 1A-C).

All of the structurally similar unlabeled ligands of the DpT series significantly ($p < 0.001$) inhibited ^{14}C-Dp44mT uptake in comparison to the control (^{14}C-Dp44mT alone; Fig. 6). In contrast, only Bp44mT and Bp4mT of the BpT series significantly ($p < 0.05$-0.001) decreased ^{14}C-Dp44mT uptake, while other analogues of the BpT series had no significant ($p > 0.05$) effect. Furthermore, Ap44mT was the only chelator of the ApT series to significantly ($p < 0.001$) decrease ^{14}C-Dp44mT uptake (Fig. 6). The ligands, Triapine® and PIH, of the thiosemicarbazone and aroylhydrazone class, respectively, had no significant ($p > 0.05$) effect on ^{14}C-Dp44mT uptake.

Unlabeled Dp44mT (100 μM) most markedly ($p < 0.001$) decreased the cellular uptake of ^{14}C-Dp44mT (25 μM) to ~40% of the control (^{14}C-Dp44mT alone; Fig. 6). Thus, the carrier/receptor involved in the uptake of Dp44mT has particularly high selectivity for Dp44mT in comparison to the range of other ligands tested. Intriguingly, a decrease in ^{14}C-Dp44mT uptake occurred consistently across all series of these α-*N*-heterocyclic chelators when the N4 atom of the unlabeled compound was saturated with the same dimethyl substituent, namely, Bp44mT, Ap44mT and Dp44mT (Fig. 6). These results suggest that ligands containing both the 2-pyridyl and 44mT moiety have affinity for the carrier/receptor site responsible for the uptake of ^{14}C-Dp44mT. It is notable that Bp44mT (Supplementary Fig. 1B) shares almost total structural identity to Dp44mT apart from the substitution of 1 nitrogen for a CH moiety (Fig. 1), but shows less activity at reducing ^{14}C-Dp44mT uptake. This observation demonstrates marked specificity in terms of the interaction of the ligand with the putative carrier/receptor.

Uptake of the Fe and Cu Complexes of the ^{14}C-Chelators: Uptake of Fe(^{14}C-Dp44mT)$_2$ does not Saturate Relative to that of Dp44mT

Molecular Pharmacology Fast Forward. Published on October 1, 2013 as DOI: 10.1124/mol.113.088393
This article has not been copyedited and formatted. The final version may differ from this version.

The uptake of the chelator complexes was also examined as numerous studies have demonstrated that thiosemicarbazone complexes are redox active, and in particular, the Cu complex of Dp44mT is more cytotoxic than the ligand alone (Jansson et al., 2010). Additionally, the anti-cancer activity of these ligands are attributed to cellular Fe- and Cu-binding (Kalinowski et al., 2007; Lovejoy et al., 2011; Merlot et al., 2013; Yuan et al., 2004). Consequently, the uptake of their Fe and Cu complexes was assessed at 37^{o}C as a function of concentration in comparison to the ligand alone (Fig. 7). Importantly, as for the studies examining ligand uptake, all experiments were performed over an incubation time of 2 h and this was particularly important to minimize any cytotoxic effects.

The uptake of the Fe(^{14}C-Dp44mT)$_2$ complex was linear (r^2 = 0.95) as a function of concentration and markedly and significantly (p < 0.01-0.001) greater than that found for the relative ligand, ^{14}C-Dp44mT (Fig. 7A). In contrast, as shown in Fig. 2A, the uptake of the ligand alone, ^{14}C-Dp44mT, demonstrated clear saturation at 5 μM (see inset, Fig. 7A). The marked uptake of the Fe complex relative to the ligand may be attributed, at least in part, to its highly lipophilic nature (Richardson et al., 2006), that results in sequestration in cellular compartments (Lovejoy et al., 2011). Notably, examination of Cu(^{14}C-Dp44mT)$_2$ uptake was attempted, but the extreme toxicity observed even after only a 2 h incubation at the concentrations utilized in Fig. 7A precluded assessment. This observation agreed well with the rapid and marked cytotoxic activity of the Cu complex relative to the Fe complex described in previous studies (Lovejoy et al., 2011).

Notably, in the studies above, there are 3 factors that indicate the complex is being taken up by cells relative to the free ligand. First, the affinity of Dp44mT for Fe is extremely high (Bernhardt et al., 2009), meaning that in the extracellular milieu that essentially there is no free ligand or metal in equilibrium, it is virtually all complexed. Second, ligand uptake alone

Molecular Pharmacology Fast Forward. Published on October 1, 2013 as DOI: 10.1124/mol.113.088393
This article has not been copyedited and formatted. The final version may differ from this version.

by cells was markedly and significantly different than its Fe complex (Fig. 7A). This observation can only be accounted for by the fact that it is the complex that is being transported into the cell and not the ligand alone. Third, ^{14}C-Dp44mT uptake saturates at 5 μM, while the uptake of the complex does not saturate and demonstrates a linear relationship as a function of concentration (Fig. 7A). These results demonstrate totally different mechanisms of uptake of ^{14}C-Dp44mT relative to its complex.

Similarly to Fe(^{14}C-Dp44mT)$_2$, the uptake of Fe(^{14}C-Bp4eT)$_2$ increased linearly as a function of concentration (r^2 = 0.98; Fig. 7B). Higher concentrations of Fe(^{14}C-Bp4eT)$_2$ (*i.e.*, > 50 μM) could not be assessed due to its highly cytotoxic nature. In addition, as evident for Fe(^{14}C-Dp44mT)$_2$, the Fe(^{14}C-Bp4eT)$_2$ complex accumulated in cells to significantly (p < 0.001) higher levels than the ligand alone (Fig. 7B). In agreement with the observation utilizing the Cu(^{14}C-Dp44mT)$_2$ complex above, the Cu(^{14}C-Bp4eT)$_2$ complex could not be assessed due to its marked cytotoxicity.

In contrast to the thiosemicarbazones above, the uptake of the Fe and Cu complexes of the aroylhydrazone, ^{14}C-PIH, could be assessed due to its markedly lower cytotoxicity (Richardson et al., 1995). This is because unlike thiosemicarbazones, aroylhydrazone ligands form complexes that are not potently redox active (Chaston et al., 2003). The uptake of the Fe(^{14}C-PIH)$_2$ complex was linear as a function of concentration (r^2 = 0.99) and was significantly (p < 0.001) greater than that found for the ligand at all concentrations above 25 μM (Fig. 7C). In contrast, as a function of concentration, uptake of Cu(^{14}C-PIH)$_2$ plateaued at 100 μM. Assessment of the saturable binding using a non-linear regression fit for a one-binding site model yielded a B_{max} value of 4.73 ± 0.43 x 10^9 ligands/cell (n = 9) and a K_d value of 34.33 ± 11.48 μM (n = 9; Table 1). The cellular accumulation of Cu(^{14}C-PIH)$_2$ was significantly (p < 0.01) higher than that of Fe(^{14}C-PIH)$_2$ at all concentrations tested except

Molecular Pharmacology Fast Forward. Published on October 1, 2013 as DOI: 10.1124/mol.113.088393
This article has not been copyedited and formatted. The final version may differ from this version.

250 μM, where no significant difference was evident (Fig. 7C).

The Effect of Temperature on the Uptake of the Fe and Cu ^{14}C-Chelator Complexes

The effect of temperature on the uptake of the Fe and Cu ^{14}C-chelator complexes and their relative ligands as a function of time was examined to determine if cellular uptake was temperature-dependent (Supplementary Fig. 3A-C). For all ligands and their Fe and Cu complexes, except Cu(^{14}C-Dp44mT)$_2$, biphasic uptake as a function of time was identified (Supplementary Fig. 3A-C). This observation implied that in the initial phase there was a rapid uptake of the ligand or complex, while in the second phase, the rate of simultaneous uptake and efflux from the cell had equilibrated, leading generally to a plateau in uptake. For some of the complexes (*e.g.*, Fe(^{14}C-Dp44mT)$_2$, Fe(^{14}C-Bp4eT)$_2$ and Cu(^{14}C-PIH)$_2$; Supplementary Fig. 3A-C), the second phase of uptake did not completely plateau, indicating gradual cellular accumulation. Intriguingly, the Cu complexes accumulated within cells to a greater extent ($p < 0.001$) than the Fe complex at 37^{o}C, which may relate to their trapping in cellular compartments such as the lysosome (Lovejoy et al., 2011).

The cellular uptake of ^{14}C-Dp44mT and ^{14}C-PIH and their complexes as a function of time was temperature-dependent, reaching higher ($p < 0.01$) intracellular concentrations at 37^{o}C than 4^{o}C (Supplementary Fig. 3A and C). As discussed above for the results in Fig. 7A, the Cu(^{14}C-Dp44mT)$_2$ complex could not be examined beyond a 30 min incubation at 37^{o}C due to cytotoxicity (Supplementary Fig. 3A). At 4^{o}C, the Cu(^{14}C-Dp44mT)$_2$ complex was far less cytotoxic than at 37^{o}C, probably because of its lower uptake at 4^{o}C, enabling a 2 h incubation (Supplementary Fig. 3A).

In contrast to ^{14}C-Dp44mT and ^{14}C-PIH, there was no significant ($p>0.05$) difference in ^{14}C-Bp4eT uptake between 4^{o}C and 37^{o}C (Supplementary Fig. 3B), as evident in previous studies (Merlot et al., 2010), demonstrating ^{14}C-Bp4eT uptake was temperature-independent.

Molecular Pharmacology Fast Forward. Published on October 1, 2013 as DOI: 10.1124/mol.113.088393
This article has not been copyedited and formatted. The final version may differ from this version.

However, in contrast, the cellular uptake of the Fe and Cu complexes of ^{14}C-Bp4eT was significantly ($p < 0.001$) higher at 37^{o}C than at 4^{o}C, indicative of a temperature-dependent mechanism (Supplementary Fig. 3B).

The Effect of Temperature on the Efflux of Fe ^{14}C-Chelator Complexes from Cells

In view of the fact that the uptake of the ^{14}C-chelator complexes by cells was greater than that of the ligand (Supplementary Fig. 3A-C), it was crucial to examine the cellular retention and efflux of the ligand and complexes. The efflux of the Fe(^{14}C-chelator)$_2$ complexes compared to ^{14}C-chelator alone was examined by a 2 h pre-incubation with ^{14}C-chelator complexes or ^{14}C-ligands alone at 37^{o}C followed by re-incubation of cells at 4^{o}C or 37^{o}C for up to 3 h (Supplementary Fig. 4A-C). In these experiments, as a result of the 2 h pre-incubation period used, the Cu(^{14}C-chelator)$_2$ complexes were too toxic to be studied.

For all chelators and their Fe complexes, a significantly ($p < 0.05$-0.001) greater release of cellular radioactivity was evident at 37^{o}C than at 4^{o}C (Supplementary Fig. 4A-C), demonstrating that the efflux of the ^{14}C-chelators and Fe(^{14}C-chelator)$_2$ complexes are highly temperature-dependent. Considering this, it is notable that active metabolic processes such as exocytosis are markedly temperature-dependent (Morgan, 1981). Hence, this observation is particularly relevant because Dp44mT uptake was mediated by a process consistent with a saturable carrier/receptor (Figs. 2-6).

Interestingly, the cellular efflux of ^{14}C-Dp44mT and its Fe complex reached similar levels at 37^{o}C with approximately 70 ± 1% and 67 ± 3% of the radiolabel being released, respectively, after 180 min (Supplementary Fig. 4A). Taking into account the higher levels of cell-bound Fe(^{14}C-Dp44mT)$_2$ (Supplementary Fig. 3A) and its similar release from cells relative to the ligand alone (Supplementary Fig. 4A), it can be concluded that there was sequestration of

Molecular Pharmacology Fast Forward. Published on October 1, 2013 as DOI: 10.1124/mol.113.088393
This article has not been copyedited and formatted. The final version may differ from this version.

Fe(^{14}C-Dp44mT)$_2$ in the cell. Furthermore, upon re-incubation, significantly ($p < 0.05$-0.001) higher levels of Bp4eT (64 ± 1% after 180 min) and PIH (73 ± 4% after 180 min) were released in comparison to their Fe complexes (29 ± 2% and 13 ± 1% at 180 min, respectively; Supplementary Fig. 4B and C). In view of the greater cellular uptake of Fe(^{14}C-Bp4eT)$_2$ and Fe(^{14}C-PIH)$_2$ (Supplementary Fig. 3B and C) and their greater retention (Supplementary Fig. 4B and C), these complexes also appear to be retained and sequestered within cells, in a similar way to Fe(^{14}C-Dp44mT)$_2$. For all complexes, this sequestration may be related to their increased lipophilicity relative to the ligands alone. This occurs due to the incorporation of the hydrophilic electron-donating groups into the coordination of Fe, decreasing their interaction with the surrounding solvent (water) and leading to greater lipophilicity (Edward et al., 1995).

In Vivo ^{14}C-Chelator Uptake

Considering the distinct saturable uptake of ^{14}C-Dp44mT in cancer cells *in vitro*, studies progressed to assessing the uptake of the ^{14}C-chelators *in vivo*. The tissue distribution of ^{14}C-Dp44mT, ^{14}C-Bp4eT and ^{14}C-PIH was investigated in BALB/c nu-nu mice bearing DMS-53 lung cancer xenografts to assess tumor uptake, bio-distribution and excretion of the chelators. This mouse model was used as DMS-53 cells readily form xenografted tumors and its response to this class of therapeutics has been well characterized by our laboratory (Lovejoy et al., 2012; Whitnall et al., 2006).

A single intravenous dose (2 mg/kg) of each ^{14}C-chelator was given 3 weeks after implantation, once the mean tumor volume reached ~400 mm^3. The mice were then sacrificed and tumor and organs collected 0.5, 1, 4 and 24 h post-injection. The amount of ^{14}C (% ID/g tissue) in major organs and tissues is presented in Fig. 8. The highest levels of ^{14}C for all three ligands were detected in organs involved in excretion, namely the liver, gallbladder, intestines, kidney and bladder (Fig. 8). In general, the levels of radioactivity in the liver, gallbladder and

Molecular Pharmacology Fast Forward. Published on October 1, 2013 as DOI: 10.1124/mol.113.088393
This article has not been copyedited and formatted. The final version may differ from this version.

small intestine peaked at 0.5-1 h and then decreased over time. In contrast, levels of ^{14}C within the large intestine generally increased and peaked at 4 or 24 h, suggesting the ^{14}C-label was progressing through the gut to the large intestine for fecal excretion (Fig. 8A-C). This latter feature of the data was most pronounced for Dp44mT. Unlike fecal excretion, renal excretion occurred more rapidly. The levels of ^{14}C peaked in the kidneys and bladder at 0.5-1 h and then declined gradually over 24 h after the injection.

Modest levels of ^{14}C were detected in the lung, spleen and heart of chelator-treated mice (Fig. 8A-C). After administration of ^{14}C-Dp44mT, 6% of the injected dose was present within the heart within 0.5 h, with this decreasing to 0.6% after 24 h (Fig. 8A). It is notable that significantly ($p < 0.01$) higher levels of ^{14}C were evident in the heart of ^{14}C-Dp44mT-treated mice (6 ± 0.86%) than ^{14}C-PIH- or ^{14}C-Bp4eT-treated mice (1% and 2.5 %, respectively) at 0.5 h (Fig. 8). Potentially, these results may be significant in understanding the cardiotoxicity in mice that was evident upon treatment with Dp44mT at high, non-optimal doses (Whitnall et al., 2006).

Of interest, for all 3 compounds, the ^{14}C level in adipose tissue (peri-renal) peaked rapidly at 0.5-1 h, and then decreased from this time point onwards (Fig. 8). Examining uptake of the 3 ligands, ^{14}C-Dp44mT appeared to be sequestered to the greatest extent in adipose tissue (Fig. 8A). In fact, after 0.5 h, significantly ($p < 0.01$) greater levels of ^{14}C-Dp44mT was identified in adipose tissue relative to mice treated with ^{14}C-Bp4eT or ^{14}C-PIH *viz.*, 18 ± 4%, 7 ± 0.6% and 3 ± 0.7% of the injected dose, respectively. Additionally, there were very minute amounts of radioactivity in brain, bone and muscle, constituting < 1%, 2% and 3%, respectively, of the administered dose at all time points (Fig. 8A-C).

After intravenous administration, the amount of radiolabel present within the blood (plasma

Molecular Pharmacology Fast Forward. Published on October 1, 2013 as DOI: 10.1124/mol.113.088393
This article has not been copyedited and formatted. The final version may differ from this version.

and blood cells) was relatively low in comparison to other tissues, demonstrating rapid drug clearance (Fig. 8A-C). Whole blood samples were separated into plasma and blood cells in order to assess the ratio of radioactivity in the whole blood and plasma. A ratio of whole blood:plasma in ideal circumstances is 1, signifying a lack of drug accumulation in blood cells (Osman et al., 1997). At 0.5 h post-dose, the blood to plasma ratio of ^{14}C-Bp4eT, ^{14}C-Dp44mT and ^{14}C-PIH was 1.18, 1.49 and 2.18, respectively (Fig. 8). This pattern was consistently observed at all time points.

In comparison to the normal tissues, and particularly the gallbladder, small intestine and large intestine, ^{14}C-ligand uptake by tumors was minor (Fig. 8A-C). However, it was relevant to note that significantly ($p < 0.05$-0.001) higher levels of ^{14}C were present in the tumor between 0.5 h to 24 h post injection of ^{14}C-Dp44mT, relative to that found after injection with ^{14}C-Bp4eT and ^{14}C-PIH (Fig. 8).

Routes of Elimination of the Ligands

In addition to tissue distribution of the ^{14}C-ligands, urine and feces were collected throughout experimental time points using metabolic cages (Fig. 9). For all compounds, the fecal ^{14}C excretion increased over the 24 h period (Fig 9A), consistent with the general increasing levels of ^{14}C evident in the large intestine and decreasing levels in the small intestine (Fig. 8). Levels of ^{14}C in the urine peaked at 0.5-1 h post-dose for all the ligands and then decreased (Fig. 9B). Notably, this observation was consistent with the decreasing levels of radiolabel present in the kidneys and bladder as a function of time (Fig. 8A-C). For mice administered ^{14}C-Bp4eT, no urine was produced in the first 0.5 h after the injection of the label, and thus, the first time point assessing urinary excretion is 1 h (Fig. 9B).

Molecular Pharmacology Fast Forward. Published on October 1, 2013 as DOI: 10.1124/mol.113.088393
This article has not been copyedited and formatted. The final version may differ from this version.

Discussion

Dp44mT Transport is via a Carrier/Receptor-Mediated Mechanism

The studies herein demonstrate that in contrast to the structurally-related ligands, Bp4eT and PIH, the cellular uptake of Dp44mT occurs *via* a carrier/receptor-mediated mechanism. This conclusion is supported by evidence demonstrating that: **(1)** ^{14}C-Dp44mT uptake as a function of concentration was saturable in 4 cell-types (Fig. 2A; Supplementary Fig. 2), while uptake of ^{14}C-Bp4eT and ^{14}C-PIH was linear (Fig. 2B,C); **(2)** ^{14}C-Dp44mT uptake was temperature- and energy-dependent (Figs. 2A, 3A-D); and **(3)** the uptake of ^{14}C-Dp44mT was subject to competitive inhibition by unlabeled Dp44mT (Fig. 4A) and also by analogues that showed very marked structural similarity (Fig. 6). With respect to temperature, at 4^{o}C, metabolically-active processes such as carrier/receptor-mediated endocytosis and exocytosis are inhibited (Morgan, 1981; Sugano et al., 2010). Thus, temperature-dependent uptake was indicative of this mechanism (Iacopetta and Morgan, 1983; Morgan, 1981; Sugano et al., 2010).

In contrast to ^{14}C-Dp44mT, the uptake of ^{14}C-Bp4eT and ^{14}C-PIH was not saturable as a function of concentration (Fig. 2A-C) and was not inhibited by metabolic inhibitors (Merlot et al., 2010), suggesting that an energy-dependent carrier/receptor was not involved in the transport of these ligands. Quantitatively, the cellular uptake of ^{14}C-Dp44mT was significantly lower than ^{14}C-Bp4eT at 37°C (*cf.* Fig. 2A and B). Furthermore, the percentage of ^{14}C-Bp4eT released from cells was lower than that of ^{14}C-Dp44mT at 37°C (Supplementary Fig. 4A,B). Together, these results demonstrate Bp4eT accumulates to a greater extent in cells than Dp44mT and may relate to its greater lipophilicity (Kalinowski et al., 2007).

The different levels of Bp4eT and Dp44mT in cells may be explained by their differing mode of uptake. The cellular uptake of Dp44mT has characteristics consistent with carrier/receptor-

Molecular Pharmacology Fast Forward. Published on October 1, 2013 as DOI: 10.1124/mol.113.088393
This article has not been copyedited and formatted. The final version may differ from this version.

mediated endocytosis (Iacopetta and Morgan, 1983; Richardson and Baker, 1990) that, due to endosomal trafficking, may direct the drug to lysosomes, which are a major target of this agent (Lovejoy et al., 2011). Additionally, greater levels of PIH were also evident in SK-N-MC cells relative to Dp44mT (Fig. 2A,C). The level of PIH did not correlate with its markedly lower anti-proliferative activity in this cell-type (PIH IC_{50} value: 75 μM; (Richardson et al., 1995)). This observation probably relates to the fact that Fe and Cu complexes of PIH are not redox-active (Chaston et al., 2003), while the redox-active Fe and Cu complexes of Dp44mT are potently cytotoxic (Lovejoy et al., 2011; Richardson et al., 2006). In contrast, lower cellular levels of PIH were evident relative to the redox-active chelator, Bp4eT, as shown previously (Merlot et al., 2010). Thus, anti-proliferative activity of the agent is not only dependent on cellular retention, but also upon its mode of transport and cytotoxic redox activity.

The saturation of Dp44mT uptake by a number of cell-types occurred at ~5-10 μM. Considering this, it is notable that this level of Dp44mT would be pharmacologically relevant in humans, as the structurally-related thiosemicarbazone, Triapine®, has been observed at similar concentrations *i.e.*, 0.5-10 μM (Chao et al., 2012; Wadler et al., 2004). Moreover, the related chelator, salicylaldehyde isonicotinoyl hydrazone (SIH), was shown to reach 100 μM in rabbit plasma upon *i.v.* administration at 10 mg/kg (Kovarikova et al., 2005). Thus, *in vivo*, Dp44mT uptake *via* the saturable carrier/receptor-mediated mechanism would be pharmacologically relevant and could occur at the concentrations predicted to result after administration.

Recently, our laboratory demonstrated hepatic phase I and II metabolism for a related DpT ligand (Stariat et al., 2013). Critically, it could be suggested that such metabolism may affect the interpretation of the ^{14}C-Dp44mT uptake results. However, 4 lines of evidence argue this

Molecular Pharmacology Fast Forward. Published on October 1, 2013 as DOI: 10.1124/mol.113.088393
This article has not been copyedited and formatted. The final version may differ from this version.

is not a significant issue. First, in contrast to our previous study that used concentrated human liver microsomes/S9 fractions (Stariat et al., 2013), the present study implemented non-hepatic tumor cells which are not rich in drug metabolizing enzymes. Hence, it is unlikely the ligands would be metabolized rapidly. Second, the experiments were specifically designed to minimize metabolism by performing uptake studies over short 30 min-2 h/37^{o}C incubations. Third, our studies compared ligand uptake at 37^{o}C to that at 4^{o}C, where no active metabolism occurs. In terms of one of the major findings in this investigation, saturable uptake of Dp44mT was still observed at 4^{o}C compared to 37^{o}C (Fig. 2A). Hence, even if metabolism occurred at 37^{o}C, major findings of the study were not affected, justifying our protocol. Fourth, competition experiments showed that receptor/carrier-mediated uptake of Dp44mT was highly specific for this ligand (Figs. 4-6). Thus, even if limited Dp44mT metabolism occurred, the metabolites would likely have little effect on uptake. Collectively, our protocol was carefully designed to minimize drug metabolism, and our studies indicate that even if this occurred, it is unlikely to markedly affect the major conclusions.

Competition for Carrier/Receptor-Binding of ^{14}C-Dp44mT with Unlabeled Precursors and Analogues

To elucidate the pharmacophore responsible for transport activity, ^{14}C-Dp44mT uptake was examined in the presence of its unlabeled synthetic precursors, DpK and 44mT (Fig. 5). Increasing concentrations of DpK or 44mT did not alter ^{14}C-Dp44mT uptake, suggesting that neither moiety is capable of binding the saturable transporter. This suggests that chemical moieties on both sub-structures are only involved when combined and are necessary for Dp44mT uptake.

A range of structurally-related thiosemicarbazones (Supplementary Fig. 1) were also examined to determine competition for the carrier/receptor-mediated transport system

Molecular Pharmacology Fast Forward. Published on October 1, 2013 as DOI: 10.1124/mol.113.088393
This article has not been copyedited and formatted. The final version may differ from this version.

responsible for Dp44mT uptake (Fig. 6). As may be expected, unlabeled Dp44mT most markedly reduced ^{14}C-Dp44mT uptake. Consistently across the ligands tested, thiosemicarbazones with a saturated terminal N4 atom (*i.e.*, Dp44mT, Bp44mT and Ap44mT) resulted in the greatest inhibition of Dp44mT uptake within their respective series and highlight the importance of this moiety in carrier/receptor-mediated uptake. Collectively, both the methyl groups at the R1 and R2 position and the coordinating pyridyl group are key structural moieties for ligand-carrier/receptor binding. Further studies are currently underway to discover the molecular identity of the Dp44mT carrier/receptor.

Saturable carriers/receptors are known for many cytotoxic drugs, including bleomycin (Pron et al., 1999), cisplatin (Ishida et al., 2002) and methotrexate (Deutsch et al., 1989). Furthermore, other thiosemicarbazones are agonists of the c-mpl thrombopoietin receptor (Duffy et al., 2002). However, it is notable that the carrier/receptor for Dp44mT was very selective for this analogue over thiosemicarbazones of the same class (Fig. 6). Consequently, it is unlikely that the c-mpl thrombopoietin receptor is involved in Dp44mT uptake as they are known to bind other thiosemicarbazones (Duffy et al., 2002).

Chelator Complexes are Sequestered in Cells

In contrast to ^{14}C-Dp44mT uptake which was saturable as a function of concentration, uptake of its Fe complex was linear (Fig. 7A), indicating a different mechanism of transport. However, a higher level of uptake of the metal complexes in contrast to the ligands was evident (Fig. 7 and Supplementary Fig. 3). This observation together with their marked redox activity may, in part, explain the greater cytotoxicity of the Cu complexes compared to the ligands (Jansson et al., 2010). The greater uptake of the complexes may be attributed to: **(1)** their increased lipophilicity *versus* the ligand (Edward et al., 1995); **(2)** differing modes of uptake; and/or **(3)** complex sequestration within cellular compartments *e.g.*, lysosomes

Molecular Pharmacology Fast Forward. Published on October 1, 2013 as DOI: 10.1124/mol.113.088393
This article has not been copyedited and formatted. The final version may differ from this version.

(Lovejoy et al., 2011). Interestingly, repeated administration of Dp44mT and a close analogue, Bp44mT to mice bearing tumor xenografts, does not lead to tumor Fe depletion, also suggesting that Fe complexes may become sequestered *in vivo* (Whitnall et al., 2006; Yu et al., 2012).

In Vivo Distribution and Excretion of ^{14}C-Chelators in Mice Bearing DMS-53 Xenografts

Due to their high lipophilicity, all three ligands were excreted in the feces with organs involved in this process being highly labeled (Fig. 8 and 9A). For all chelators, radioactivity peaked in the feces 24 h after administration. In contrast, renal excretion occurred more rapidly with levels of ^{14}C in urine peaking at 0.5-1 h post-injection of ^{14}C-ligand with the quantity of radiolabel declining over time (Fig. 9B). This is consistent with the decreasing levels of radiolabel present in excretory tissue, namely the kidneys and bladder (Fig. 8).

Interestingly, at all time points, there was little uptake of the ^{14}C-chelators in the brain, bone and muscle of mice (Fig. 8A-C). This agrees with the limited toxicity found in these organs after treatment (Lovejoy et al., 2012; Whitnall et al., 2006; Yu et al., 2012). Only a minor proportion of ^{14}C-labeled ligands were detected in the tumors, with significantly more ^{14}C-Dp44mT being detected relative to the other ligands (Fig. 8A). This difference may be indicative of the anti-cancer efficacy of the chelators *in vivo*.

Collectively, Dp44mT is transported into cells by a saturable carrier/receptor-mediated mechanism. Competition experiments demonstrated that the saturated N4 structural moiety and the coordinating pyridyl substituent were critical for carrier/receptor recognition. Studies assessing the tissue distribution of ^{14}C-Dp44mT injected intravenously into mice bearing xenografted tumors, demonstrated the ^{14}C label was primarily identified in organs associated

with fecal and urinary excretion. Collectively, these results have clinical implications for understanding the bioavailability and uptake of Dp44mT *in vivo*.

Acknowledgments

Ms Danae Sharp is thanked for her assistance with the animal study.

Author Contribution

Participated in research design: Merlot, Richardson and Kalinowski.

Conducted experiments: Merlot, Pantarat, Menezes, Sahni and Kalinowski.

Performed data analysis: Merlot, Pantarat, Menezes, Sahni and Kalinowski.

Wrote or contributed to the writing of the manuscript: Merlot, Richardson and Kalinowski.

Molecular Pharmacology Fast Forward. Published on October 1, 2013 as DOI: 10.1124/mol.113.088393
This article has not been copyedited and formatted. The final version may differ from this version.

References

Baker E, Richardson D, Gross S and Ponka P (1992) Evaluation of the iron chelation potential of hydrazones of pyridoxal, salicylaldehyde and 2-hydroxy-1-naphthylaldehyde using the hepatocyte in culture. *Hepatology* **15:** 492-501.

Baker E, Vitolo ML and Webb J (1985) Iron chelation by pyridoxal isonicotinoyl hydrazone and analogues in hepatocytes in culture. *Biochem Pharmacol* **34:** 3011-3017.

Balsari A, Tortoreto M, Besusso D, Petrangolini G, Sfondrini L, Maggi R, Menard S and Pratesi G (2004) Combination of a CpG-oligodeoxynucleotide and a topoisomerase I inhibitor in the therapy of human tumour xenografts. *Eur J Cancer* **40:** 1275-1281.

Bernhardt PV, Sharpe PC, Islam M, Lovejoy DB, Kalinowski DS and Richardson DR (2009) Iron chelators of the dipyridylketone thiosemicarbazone class: precomplexation and transmetalation effects on anticancer activity. *J Med Chem* **52:** 407-415.

Buss JL, Torti FM and Torti SV (2003) The role of iron chelation in cancer therapy. *Curr Med Chem* **10:** 1021-1034.

Chao J, Synold TW, Morgan RJ, Jr., Kunos C, Longmate J, Lenz HJ, Lim D, Shibata S, Chung V, Stoller RG, Belani CP, Gandara DR, McNamara M, Gitlitz BJ, Lau DH, Ramalingam SS, Davies A, Espinoza-Delgado I, Newman EM and Yen Y (2012) A phase I and pharmacokinetic study of oral 3-aminopyridine-2-carboxaldehyde thiosemicarbazone (3-AP, NSC #663249) in the treatment of advanced-stage solid cancers: a California Cancer Consortium Study. *Cancer Chemother Pharmacol* **69:** 835-843.

Chaston TB, Lovejoy DB, Watts RN and Richardson DR (2003) Examination of the antiproliferative activity of iron chelators: multiple cellular targets and the different mechanism of action of triapine compared with desferrioxamine and the potent

pyridoxal isonicotinoyl hydrazone analogue 311. *Clin Cancer Res* **9:** 402-414.

Chung MC-M (1984) Structure and function of transferrin. *Biochem Educ* **12:** 146-154.

Ciechanover A, Schwartz AL and Lodish HF (1983) The asialoglycoprotein receptor internalizes and recycles independently of the transferrin and insulin receptors. *Cell* **32:** 267-275.

Deutsch JC, Elwood PC, Portillo RM, Macey MG and Kolhouse JF (1989) Role of the membrane-associated folate binding protein (folate receptor) in methotrexate transport by human KB cells. *Arch Biochem Biophys* **274:** 327-337.

Duffy KJ, Shaw AN, Delorme E, Dillon SB, Erickson-Miller C, Giampa L, Huang Y, Keenan RM, Lamb P, Liu N, Miller SG, Price AT, Rosen J, Smith H, Wiggall KJ, Zhang L and Luengo JI (2002) Identification of a pharmacophore for thrombopoietic activity of small, non-peptidyl molecules. 1. Discovery and optimization of salicylaldehyde thiosemicarbazone thrombopoietin mimics. *J Med Chem* **45:** 3573-3575.

Edward JT, Ponka P and Richardson DR (1995) Partition coefficients of the iron(III) complexes of pyridoxal isonicotinoyl hydrazone and its analogs and the correlation to iron chelation efficacy. *Biometals* **8:** 207-217.

Elford HL, Freese M, Passamani E and Morris HP (1970) Ribonucleotide reductase and cell proliferation. I. Variations of ribonucleotide reductase activity with tumor growth rate in a series of rat hepatomas. *J Biol Chem* **245:** 5228-5233.

Hanahan D and Weinberg RA (2011) Hallmarks of cancer: the next generation. *Cell* **144:** 646-674.

Harding C, Heuser J and Stahl P (1983) Receptor-mediated endocytosis of transferrin and recycling of the transferrin receptor in rat reticulocytes. *J Cell Biol* **97:** 329-339.

Henderson GB and Zevely EM (1984) Transport routes utilized by L1210 cells for the influx and efflux of methotrexate. *J Biol Chem* **259:** 1526-1531.

Hsieh HS and Frieden E (1975) Evidence for ceruloplasmin as a copper transport protein.

Biochem Biophys Res Commun **67:** 1326-1331.

Iacopetta BJ and Morgan EH (1983) The kinetics of transferrin endocytosis and iron uptake from transferrin in rabbit reticulocytes. *J Biol Chem* **258:** 9108-9115.

Ishida S, Lee J, Thiele DJ and Herskowitz I (2002) Uptake of the anticancer drug cisplatin mediated by the copper transporter Ctr1 in yeast and mammals. *Proc Natl Acad Sci U S A* **99:** 14298-14302.

Jansson PJ, Sharpe PC, Bernhardt PV and Richardson DR (2010) Novel thiosemicarbazones of the ApT and DpT series and their copper complexes: identification of pronounced redox activity and characterization of their antitumor activity. *J Med Chem* **53:** 5759-5769.

Kalinowski DS and Richardson DR (2005) The evolution of iron chelators for the treatment of iron overload disease and cancer. *Pharmacol Rev* **57:** 547-583.

Kalinowski DS, Yu Y, Sharpe PC, Islam M, Liao YT, Lovejoy DB, Kumar N, Bernhardt PV and Richardson DR (2007) Design, synthesis, and characterization of novel iron chelators: structure-activity relationships of the 2-benzoylpyridine thiosemicarbazone series and their 3-nitrobenzoyl analogues as potent antitumor agents. *J Med Chem* **50:** 3716-3729.

Kovacevic Z, Chikhani S, Lovejoy DB and Richardson DR (2011) Novel thiosemicarbazone iron chelators induce up-regulation and phosphorylation of the metastasis suppressor N-myc down-stream regulated gene 1: a new strategy for the treatment of pancreatic cancer. *Mol Pharmacol* **80:** 598-609.

Kovarikova P, Klimes J, Sterba M, Popelova O, Mokry M, Gersl V and Ponka P (2005) Development of high-performance liquid chromatographic determination of salicylaldehyde isonicotinoyl hydrazone in rabbit plasma and application of this method to an in vivo study. *J Sep Sci* **28:** 1300-1306.

Le NT and Richardson DR (2004) Iron chelators with high antiproliferative activity up-

regulate the expression of a growth inhibitory and metastasis suppressor gene: a link between iron metabolism and proliferation. *Blood* **104:** 2967-2975.

Liu W, Xing F, Iiizumi-Gairani M, Okuda H, Watabe M, Pai SK, Pandey PR, Hirota S, Kobayashi A, Mo YY, Fukuda K, Li Y and Watabe K (2012) N-myc downstream regulated gene 1 modulates Wnt-beta-catenin signalling and pleiotropically suppresses metastasis. *EMBO Mol Med* **4:** 93-108.

Lovejoy DB, Jansson PJ, Brunk UT, Wong J, Ponka P and Richardson DR (2011) Antitumor activity of metal-chelating compound Dp44mT is mediated by formation of a redox-active copper complex that accumulates in lysosomes. *Cancer Res* **71:** 5871-5880.

Lovejoy DB, Sharp DM, Seebacher N, Obeidy P, Prichard T, Stefani C, Basha MT, Sharpe PC, Jansson PJ, Kalinowski DS, Bernhardt PV and Richardson DR (2012) Novel second-generation di-2-pyridylketone thiosemicarbazones show synergism with standard chemotherapeutics and demonstrate potent activity against lung cancer xenografts after oral and intravenous administration in vivo. *J Med Chem* **55:** 7230-7244.

Mc Farlane AS (1958) Efficient trace-labelling of proteins with iodine. *Nature* **182:** 53.

Merlot AM, Kalinowski DS and Richardson DR (2013) Novel Chelators for Cancer Treatment: Where Are We Now? *Antioxid Redox Signal* **18:** 973-1006.

Merlot AM, Pantarat N, Lovejoy DB, Kalinowski DS and Richardson DR (2010) Membrane transport and intracellular sequestration of novel thiosemicarbazone chelators for the treatment of cancer. *Mol Pharmacol* **78:** 675-684.

Moore PA (1981) Preparation of whole blood for liquid scintillation counting. *Clin Chem* **27:** 609-611.

Morgan EH (1981) Transferrin, biochemistry, physiology, and clinical significance. *Molec Aspects Med* **4:** 1-123.

Morgan EH and Baker E (1969) The effect of metabolic inhibitors on transferrin and iron

uptake and transferrin release from reticulocytes. *Biochim Biophys Acta* **184:** 442-454.

Mulford CA and Lodish HF (1988) Endocytosis of the transferrin receptor is altered during differentiation of murine erythroleukemic cells. *J Biol Chem* **263:** 5455–5461.

Noulsri E, Richardson DR, Lerdwana S, Fucharoen S, Yamagishi T, Kalinowski DS and Pattanapanyasat K (2009) Antitumor activity and mechanism of action of the iron chelator, Dp44mT, against leukemic cells. *Am J Hematol* **84:** 170-176.

Osman S, Luthra SK, Brady F, Hume SP, Brown G, Harte RJ, Matthews JC, Denny WA, Baguley BC, Jones T and Price PM (1997) Studies on the metabolism of the novel antitumor agent [N-methyl-11C]N-[2-(dimethylamino)ethyl]acridine-4-carboxamide in rats and humans prior to phase I clinical trials. *Cancer Res* **57:** 2172-2180.

Pinnix ZK, Miller LD, Wang W, D'Agostino R, Jr., Kute T, Willingham MC, Hatcher H, Tesfay L, Sui G, Di X, Torti SV and Torti FM (2010) Ferroportin and iron regulation in breast cancer progression and prognosis. *Sci Transl Med* **2:** 43ra56.

Porter JB, Gyparaki M, Burke LC, Huehns ER, Sarpong P, Saez V and Hider RC (1988) Iron mobilization from hepatocyte monolayer cultures by chelators: the importance of membrane permeability and the iron-binding constant. *Blood* **72:** 1497-1503.

Pron G, Mahrour N, Orlowski S, Tounekti O, Poddevin B, Belehradek J, Jr. and Mir LM (1999) Internalisation of the bleomycin molecules responsible for bleomycin toxicity: a receptor-mediated endocytosis mechanism. *Biochem Pharmacol* **57:** 45-56.

Qian ZM and Morgan EH (1991) Effect of metabolic inhibitors on uptake of non-transferrin-bound iron by reticulocytes. *Biochim Biophys Acta* **1073:** 456-462.

Rao VA, Klein SR, Agama KK, Toyoda E, Adachi N, Pommier Y and Shacter EB (2009) The iron chelator Dp44mT causes DNA damage and selective inhibition of topoisomerase IIalpha in breast cancer cells. *Cancer Res* **69:** 948-957.

Richardson D, Ponka P and Baker E (1994) The effect of the iron(III) chelator, desferrioxamine, on iron and transferrin uptake by the human malignant melanoma

cell. *Cancer Res* **54:** 685-689.

Richardson DR (1997) Mobilization of iron from neoplastic cells by some iron chelators is an energy-dependent process. *Biochim Biophys Acta* **1320:** 45-57.

Richardson DR and Baker E (1990) The uptake of iron and transferrin by the human malignant melanoma cell. *Biochim Biophys Acta* **1053:** 1-12.

Richardson DR, Kalinowski DS, Richardson V, Sharpe PC, Lovejoy DB, Islam M and Bernhardt PV (2009) 2-Acetylpyridine thiosemicarbazones are potent iron chelators and antiproliferative agents: redox activity, iron complexation and characterization of their antitumor activity. *J Med Chem* **52:** 1459-1470.

Richardson DR and Ponka P (1994) The iron metabolism of the human neuroblastoma cell: lack of relationship between the efficacy of iron chelation and the inhibition of DNA synthesis. *J Lab Clin Med* **124:** 660-671.

Richardson DR, Sharpe PC, Lovejoy DB, Senaratne D, Kalinowski DS, Islam M and Bernhardt PV (2006) Dipyridyl thiosemicarbazone chelators with potent and selective antitumor activity form iron complexes with redox activity. *J Med Chem* **49:** 6510-6521.

Richardson DR, Tran EH and Ponka P (1995) The potential of iron chelators of the pyridoxal isonicotinoyl hydrazone class as effective antiproliferative agents. *Blood* **86:** 4295-4306.

Seymour GJ, Walsh MD, Lavin MF, Strutton G and Gardiner RA (1987) Transferrin receptor expression by human bladder transitional cell carcinomas. *Urol Res* **15:** 341-344.

Soyer HP, Smolle J, Torne R and Kerl H (1987) Transferrin receptor expression in normal skin and in various cutaneous tumors. *J Cutan Pathol* **14:** 1-5.

Stariat J, Kovarikova P, Kucera R, Klimes J, Kalinowski DS, Richardson DR and Ketola RA (2013) Identification of in vitro metabolites of the novel anti-tumor thiosemicarbazone, DpC, using ultra-high performance liquid chromatography-

quadrupole-time-of-flight mass spectrometry. *Anal Bioanal Chem* **405:** 1651-1661.

Sugano K, Kansy M, Artursson P, Avdeef A, Bendels S, Di L, Ecker GF, Faller B, Fischer H, Gerebtzoff G, Lennernaes H and Senner F (2010) Coexistence of passive and carrier-mediated processes in drug transport. *Nat Rev Drug Discov* **9:** 597-614.

Takeda E and Weber G (1981) Role of ribonucleotide reductase in expression in the neoplastic program. *Life Sci* **28:** 1007-1014.

Tian J, Peehl DM, Zheng W and Knox SJ (2010) Anti-tumor and radiosensitization activities of the iron chelator HDp44mT are mediated by effects on intracellular redox status. *Cancer Lett* **298:** 231-237.

Wadler S, Makower D, Clairmont C, Lambert P, Fehn K and Sznol M (2004) Phase I and pharmacokinetic study of the ribonucleotide reductase inhibitor, 3-aminopyridine-2-carboxaldehyde thiosemicarbazone, administered by 96-hour intravenous continuous infusion. *J Clin Oncol* **22:** 1553-1563.

Whitnall M, Howard J, Ponka P and Richardson DR (2006) A class of iron chelators with a wide spectrum of potent antitumor activity that overcomes resistance to chemotherapeutics. *Proc Natl Acad Sci U S A* **103:** 14901-14906.

Yu Y, Suryo Rahmanto Y, Hawkins CL and Richardson DR (2011) The potent and novel thiosemicarbazone chelators di-2-pyridylketone-4,4-dimethyl-3-thiosemicarbazone and 2-benzoylpyridine-4,4-dimethyl-3-thiosemicarbazone affect crucial thiol systems required for ribonucleotide reductase activity. *Mol Pharmacol* **79:** 921-931.

Yu Y, Suryo Rahmanto Y and Richardson DR (2012) Bp44mT: an orally active iron chelator of the thiosemicarbazone class with potent anti-tumour efficacy. *Br J Pharmacol* **165:** 148-166.

Yuan J, Lovejoy DB and Richardson DR (2004) Novel di-2-pyridyl-derived iron chelators with marked and selective antitumor activity: in vitro and in vivo assessment. *Blood* **104:** 1450-1458.

Molecular Pharmacology Fast Forward. Published on October 1, 2013 as DOI: 10.1124/mol.113.088393
This article has not been copyedited and formatted. The final version may differ from this version.

Footnotes

This work was supported by the National Health and Medical Research Council of Australia to D.R.R. and D.S.K. [Project Grant #1021607, #1021601 and #1048972; Senior Principal Research Fellowship #571123]; and Cancer Institute New South Wales [Early Career Development Fellowship 08/ECF/1-30]. A.M.M. sincerely appreciates a Bob and Nancy Edwards Postgraduate Scholarship from the Sydney Medical School, University of Sydney.

D.S.K. and D.R.R. contributed equally as co-corresponding senior authors.

Reprint requests to be sent to Prof. Des R. Richardson (Molecular Pharmacology and Pathology Program, Department of Pathology, Blackburn Building D06, University of Sydney, NSW 2006, Australia). Email: d.richardson@med.usyd.edu.au.

The authors declare no conflict of interest.

Molecular Pharmacology Fast Forward. Published on October 1, 2013 as DOI: 10.1124/mol.113.088393
This article has not been copyedited and formatted. The final version may differ from this version.

Figure Legends

Figure 1. Line drawings of the chemical structures of the iron chelators: di-2-pyridylketone 4,4-dimethyl-3-thiosemicarbazone (Dp44mT), 2-benzoylpyridine 4-ethyl-3-thiosemicarbazone (Bp4eT), pyridoxal isonicotinoyl hydrazone (PIH) and Triapine®. Asterix (*) indicates position of the ^{14}C-label.

Figure 2. The uptake of: **(A)** ^{14}C-Dp44mT, **(B)** ^{14}C-Bp4eT and **(C)** ^{14}C-PIH by SK-N-MC neuroepithelioma cells as a function of concentration at 4^{o}C and 37^{o}C. The cells were incubated in media containing ^{14}C-Dp44mT (0.1-100 μM), ^{14}C-Bp4eT (5-250 μM) or ^{14}C-PIH (5-250 μM) for 120 min at 4^{o}C or 37^{o}C. The cells were then placed on ice, washed 4 times using ice-cold PBS, suspended in PBS (1 mL) and the radioactivity was quantified. Results are expressed as mean ± S.E.M. (3 experiments).

Figure 3. Incubation of SK-N-MC cells with the metabolic inhibitors, NaN_3 (30 mM) or NaCN (5 mM), significantly reduced: **(A)** ^{14}C-Dp44mT (25 μM) uptake; **(B)** cellular ATP levels; **(C)** ^{59}Fe uptake or **(D)**^{125}I-transferrin uptake by cells from ^{59}Fe-^{125}I-transferrin ([Fe] = 0.75 μM; [transferrin] = 0.375 μM). Cells were preincubated with inhibitors or media alone for 30 min/37°C. The media were then removed and replaced with new media containing ^{14}C-Dp44mT or ^{59}Fe-^{125}I-transferrin in the presence or absence of inhibitors, and incubated for 60 min/37°C. The cells were then washed and processed for quantification of ^{14}C, ATP levels, ^{59}Fe or ^{125}I. Results are expressed as % control ± S.E.M. (3 experiments). **, $p < 0.01$; ***, $p < 0.001$ *versus* control.

Figure 4. The cellular uptake of: **(A)** ^{14}C-Dp44mT, **(B)** ^{14}C-Bp4eT and **(C)** ^{14}C-PIH in the

Molecular Pharmacology Fast Forward. Published on October 1, 2013 as DOI: 10.1124/mol.113.088393
This article has not been copyedited and formatted. The final version may differ from this version.

presence of unlabeled Dp44mT, Bp4eT or PIH, respectively, in SK-N-MC cells. Cells were incubated in medium with ^{14}C-Dp44mT, ^{14}C-Bp4eT or ^{14}C-PIH (25 μM) in the absence (control) or presence of unlabeled Dp44mT, Bp4eT or PIH (2.5-250 μM), respectively, for 30 min at 37^{o}C. The cells were then placed on ice and washed 4 times with ice-cold PBS and the radioactivity was quantified. Results are mean ± S.E.M. (3 experiments) and are expressed as a % of the control. ***, $p < 0.001$ *versus* control ^{14}C-Dp44mT or ^{14}C-Bp4eT alone.

Figure 5. The cellular uptake of ^{14}C-Dp44mT in the presence of: **(A)** Dp44mT, or its unlabeled precursors: **(B)** di-2-pyridylketone (DpK), or **(C)** 4,4-dimethyl-3-thiosemicarbazide (44mT), by SK-N-MC cells. The cells were incubated with ^{14}C-Dp44mT (25 μM) in the presence of increasing concentrations of unlabeled Dp44mT or its unlabeled precursors, DpK or 44mT (2.5-250 μM), for 30 min at 37^{o}C. Cells were the washed 4 times on ice with ice-cold PBS and the radioactivity was quantified. Chemical structures of each compound are shown as insets in the figure. Results are mean ± S.E.M. (3 experiments) and are expressed as a % of the control. ***, $p < 0.001$, *versus* uptake of ^{14}C-Dp44mT alone (*i.e.*, in the absence of any unlabeled Dp44mT).

Figure 6. The effect of unlabeled structurally-related ligands on the cellular uptake of ^{14}C-Dp44mT in SK-N-MC cells. Cells were incubated with ^{14}C-Dp44mT (25 μM) in the presence of a range of structurally-related unlabeled chelators (100 μM) from the DpT series (DpT, Dp4mT, Dp44mT, Dp4eT, Dp4aT, Dp4pT and DpC), the BpT series (BpT, Bp4mT, Bp44mT, Bp4eT, and Bp4aT), the ApT series (ApT, Ap4mT, Ap44mT, Ap4eT and Ap4pT), Triapine® or PIH for 30 min at 37^{o}C. Cells were then washed 4 times on ice with ice-cold PBS and the radioactivity was quantified. General chemical structures of each compound are shown in the figure. Results are mean ± S.E.M. (3 experiments) and are expressed as a % of the control (^{14}C-Dp44mT alone). *, $p < 0.05$; ***, $p < 0.001$, *versus* uptake of ^{14}C-Dp44mT alone (*i.e.*, in

Molecular Pharmacology Fast Forward. Published on October 1, 2013 as DOI: 10.1124/mol.113.088393
This article has not been copyedited and formatted. The final version may differ from this version.

the absence of any unlabeled competitor).

Figure 7. The uptake of the Fe and Cu complexes of the ^{14}C-chelators as a function of concentration by SK-N-MC cells relative to the ligands alone. The cells were incubated in media containing: **(A)** ^{14}C-Dp44mT or Fe(^{14}C-Dp44mT)$_2$ (0.1-125 μM); **(B)** ^{14}C-Bp4eT or Fe(^{14}C-Bp4eT)$_2$ (5-250 μM); or **(C)** ^{14}C-PIH, Fe(^{14}C-PIH)$_2$ or Cu(^{14}C-PIH)$_2$ (5-250 μM) for 120 min at 4^{o}C or 37^{o}C. Cells were then washed 4 times on ice with ice-cold PBS and the radioactivity was quantified. The inset in **(A)** shows the relative uptake of ^{14}C-Dp44mT (scale: molecules chelator/cell x 10^7) which is far lower than the uptake of its Fe complex (scale: molecules chelator/cell x 10^9). Results are mean ± S.E.M. (4 experiments).

Figure 8. Tissue distribution of: **(A)** ^{14}C-Dp44mT, **(B)** ^{14}C-Bp4eT and **(C)** ^{14}C-PIH in BALB/c nu/nu mice bearing a DMS-53 tumor xenograft. Radiolabeled ^{14}C-Dp44mT, ^{14}C-Bp4eT or ^{14}C-PIH was administered intravenously *via* the tail vein to yield a final dose of 2 mg/kg and final specific activity of 1 μCi. At 0.5, 1, 4 and 24 h post-administration, the heart, lungs, brain, liver, gallbladder, small intestine, large intestine, kidney, bladder, spleen, peri-renal adipose tissue, skeletal muscle, bone (left femur), tumor, plasma and blood cells were collected and radioactivity was quantified. Values for each time point were expressed as % of injected dose (ID)/g of tissue and as mean ± S.E.M. (n = 4 mice).

Figure 9. The ^{14}C levels in feces and urine excreted by BALB/c nu/nu mice bearing a DMS-53 tumor xenograft administered either: ^{14}C-Dp44mT, ^{14}C-Bp4eT or ^{14}C-PIH (2 mg/kg) *via* the tail vein using the same protocol described in Figure 9. **(A)** Fecal excretion collected from mice (n = 4) in metabolic cages during the 0.5, 1, 4 and 24 h period post-injection. **(B)** Urine collected from mice (n = 4) in metabolic cages during the 0.5, 1, 4 and 24 h period post-injection. Results represent combined excretion from the 4 mice/cage.

Molecular Pharmacology Fast Forward. Published on October 1, 2013 as DOI: 10.1124/mol.113.088393
This article has not been copyedited and formatted. The final version may differ from this version.

Table 1: B_{max}, maximum number of binding sites, and K_d, equilibrium constant, from analysis of saturable uptake experiments as a function of concentration of ^{14}C-Dp44mT and Cu(^{14}C-PIH)$_2$ using SK-N-MC neuroepithelioma cells. Results are Mean ± SD (n = 9).

Chelator	*Temperature*	*B_{max} (molecules of chelator/cell)*	*K_d (μM)*	*% internalized*
Dp44mT	**37°C**	4.28 ± 0.26 x 10^7	2.45 ± 0.67	62 ± 16%
	4°C	2.49 ± 0.13 x 10^7	4.71 ± 1.00	
Cu(PIH)$_2$	**37°C**	4.73 ± 0.43 x 10^9	34.33 ± 11.48	---

Molecular Pharmacology Fast Forward. Published on October 1, 2013 as DOI: 10.1124/mol.113.088393
This article has not been copyedited and formatted. The final version may differ from this version.

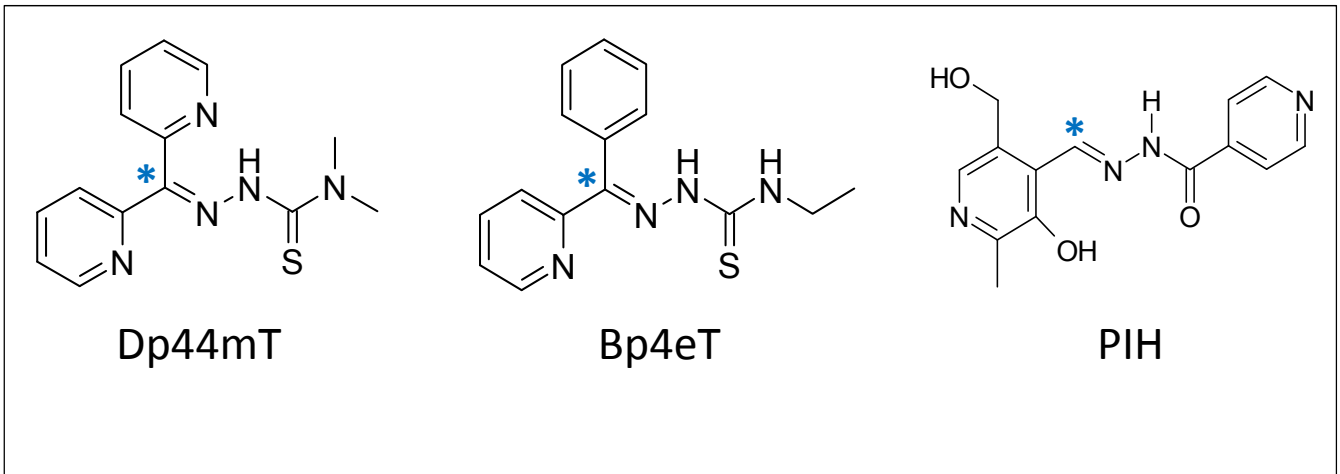

Figure 1

Molecular Pharmacology Fast Forward. Published on October 1, 2013 as DOI: 10.1124/mol.113.088393
This article has not been copyedited and formatted. The final version may differ from this version.

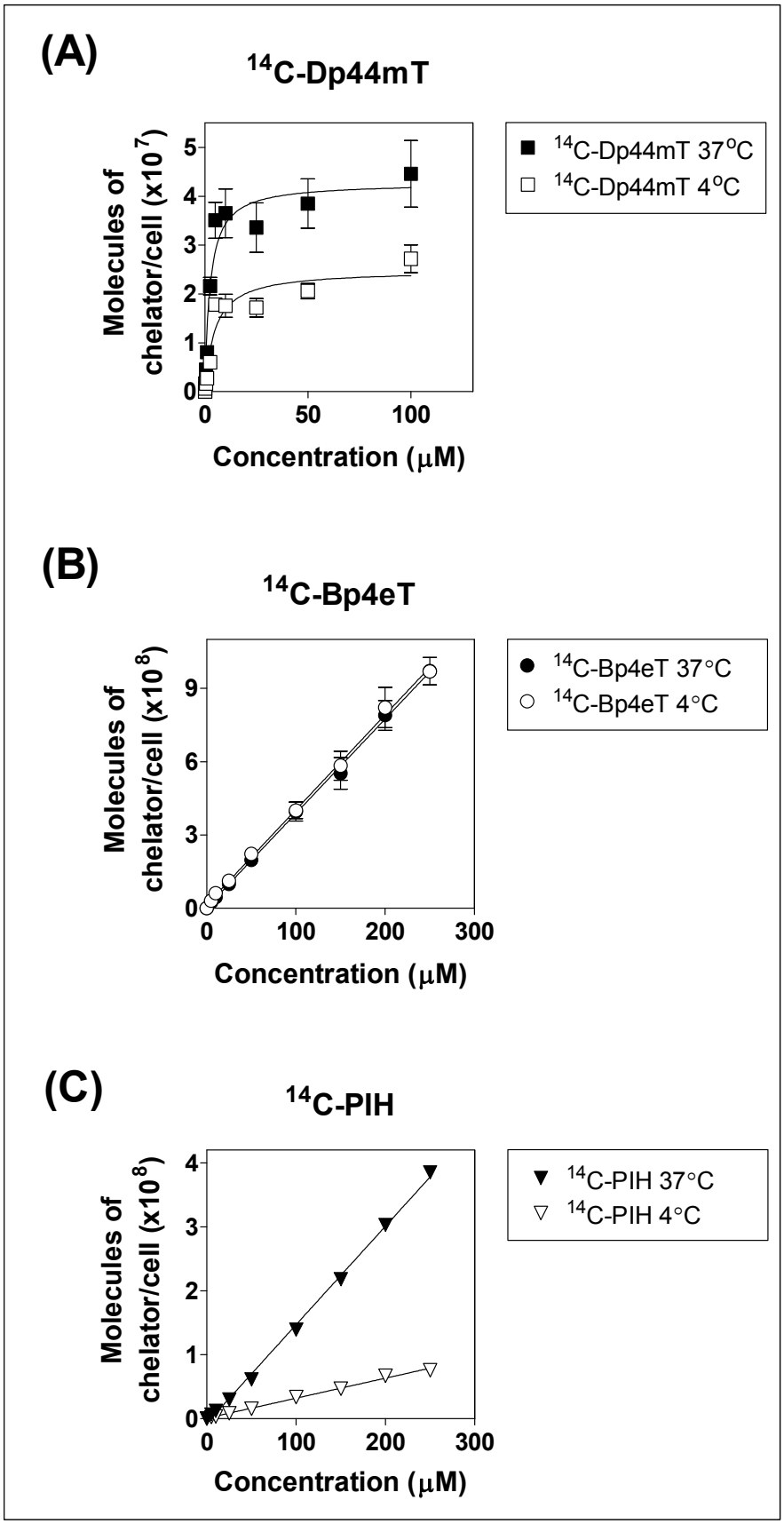

Figure 2

Molecular Pharmacology Fast Forward. Published on October 1, 2013 as DOI: 10.1124/mol.113.088393
This article has not been copyedited and formatted. The final version may differ from this version.

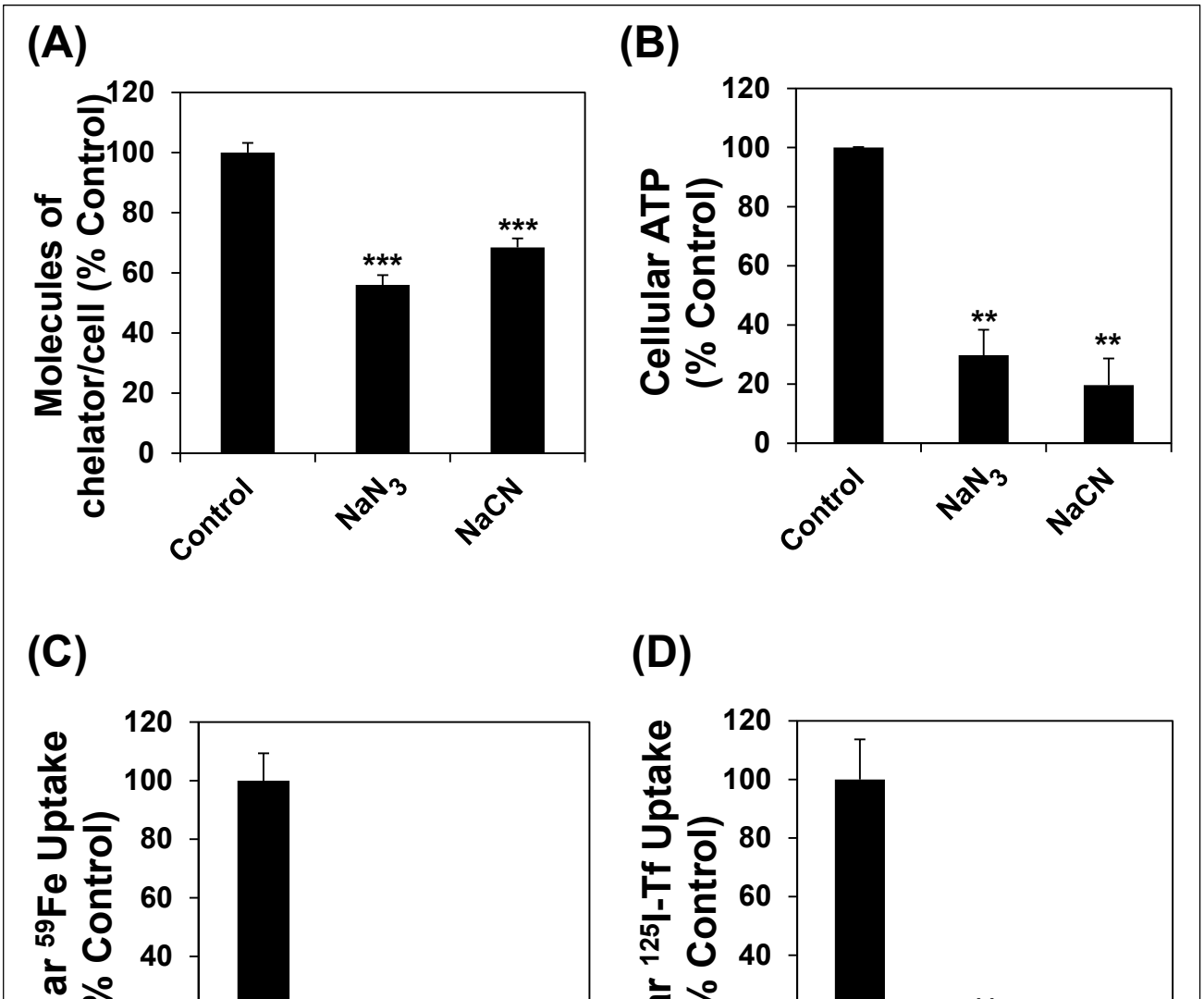

Figure 3

Molecular Pharmacology Fast Forward. Published on October 1, 2013 as DOI: 10.1124/mol.113.088393
This article has not been copyedited and formatted. The final version may differ from this version.

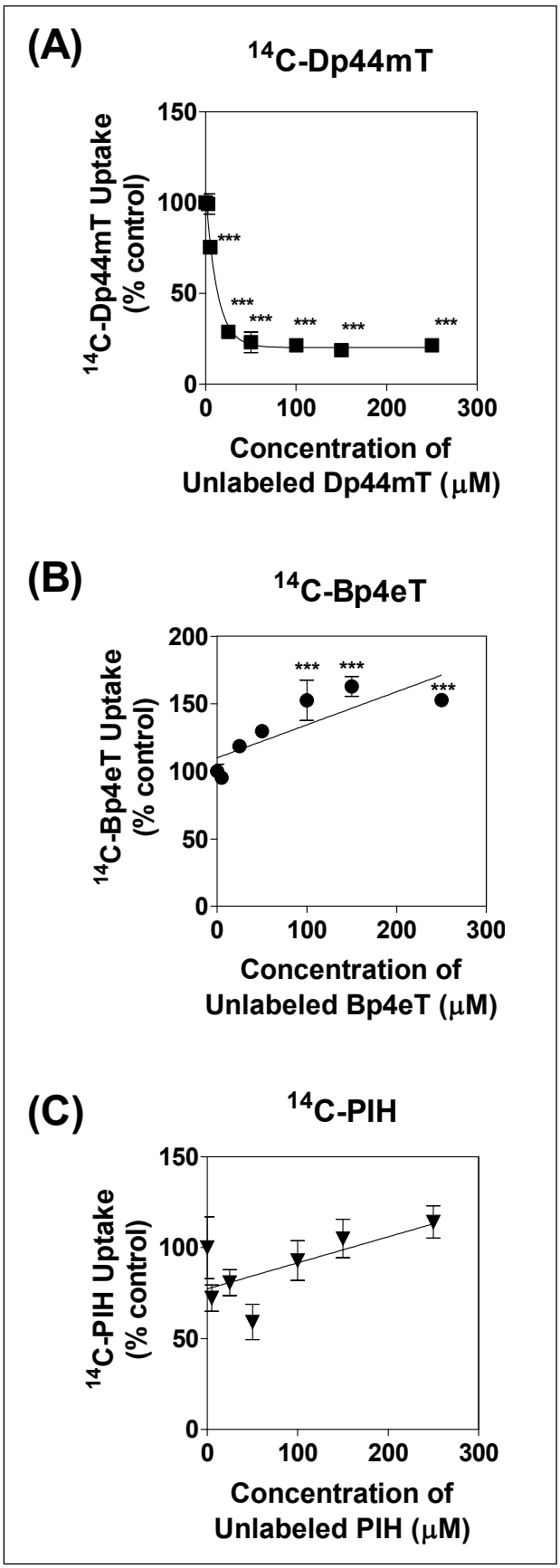

Figure 4

Molecular Pharmacology Fast Forward. Published on October 1, 2013 as DOI: 10.1124/mol.113.088393
This article has not been copyedited and formatted. The final version may differ from this version.

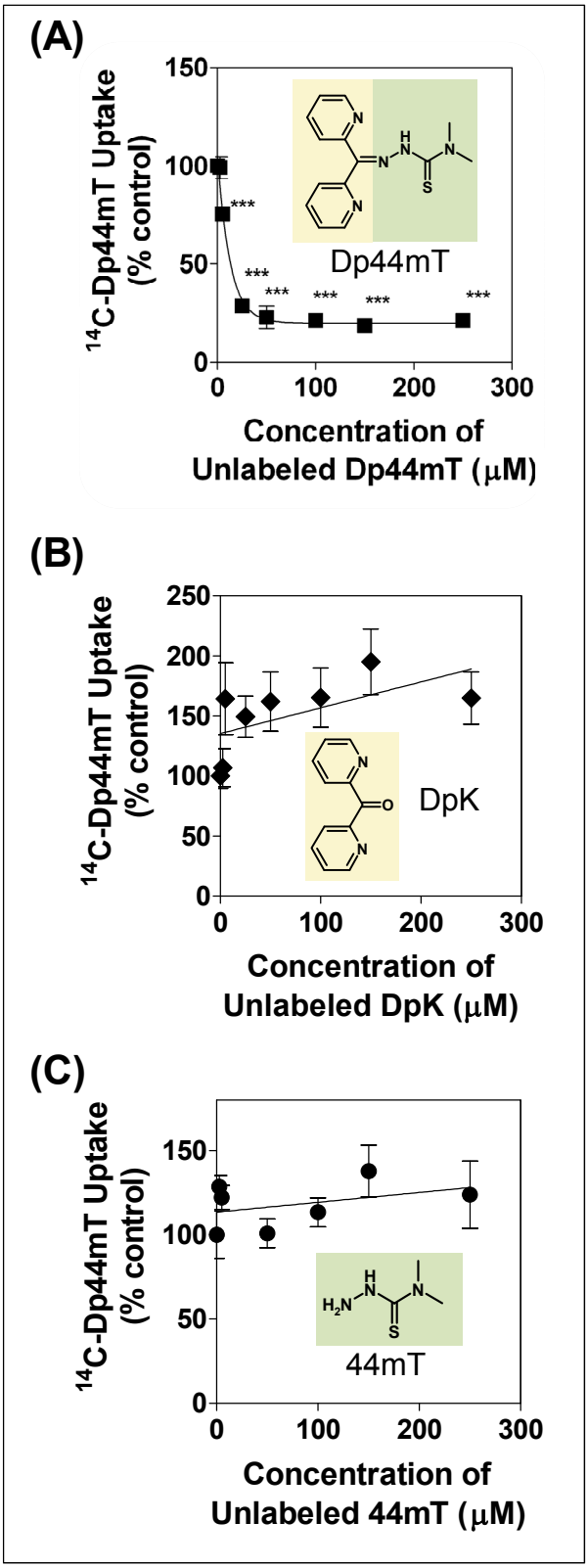

Figure 5

Molecular Pharmacology Fast Forward. Published on October 1, 2013 as DOI: 10.1124/mol.113.088393
This article has not been copyedited and formatted. The final version may differ from this version.

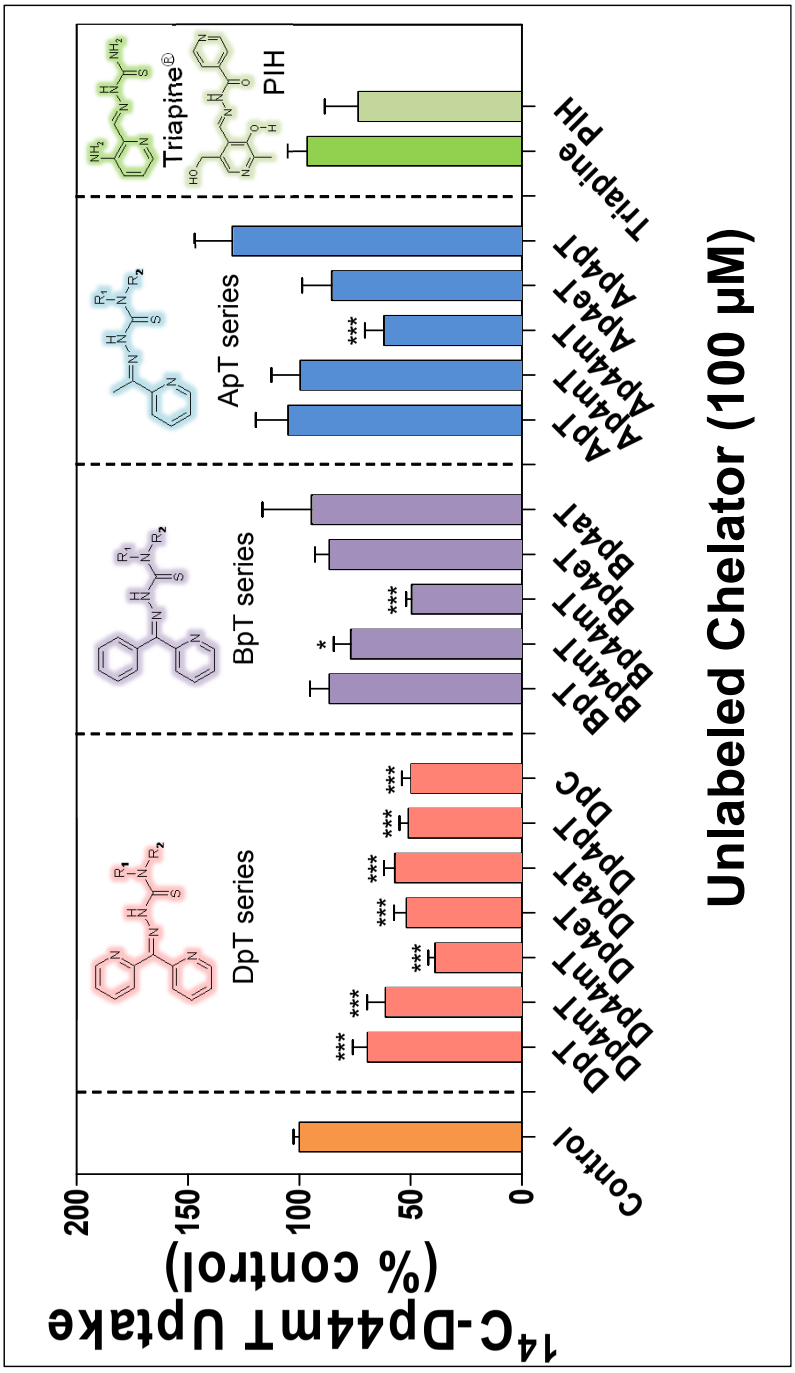

Figure 6

Molecular Pharmacology Fast Forward. Published on October 1, 2013 as DOI: 10.1124/mol.113.088393
This article has not been copyedited and formatted. The final version may differ from this version.

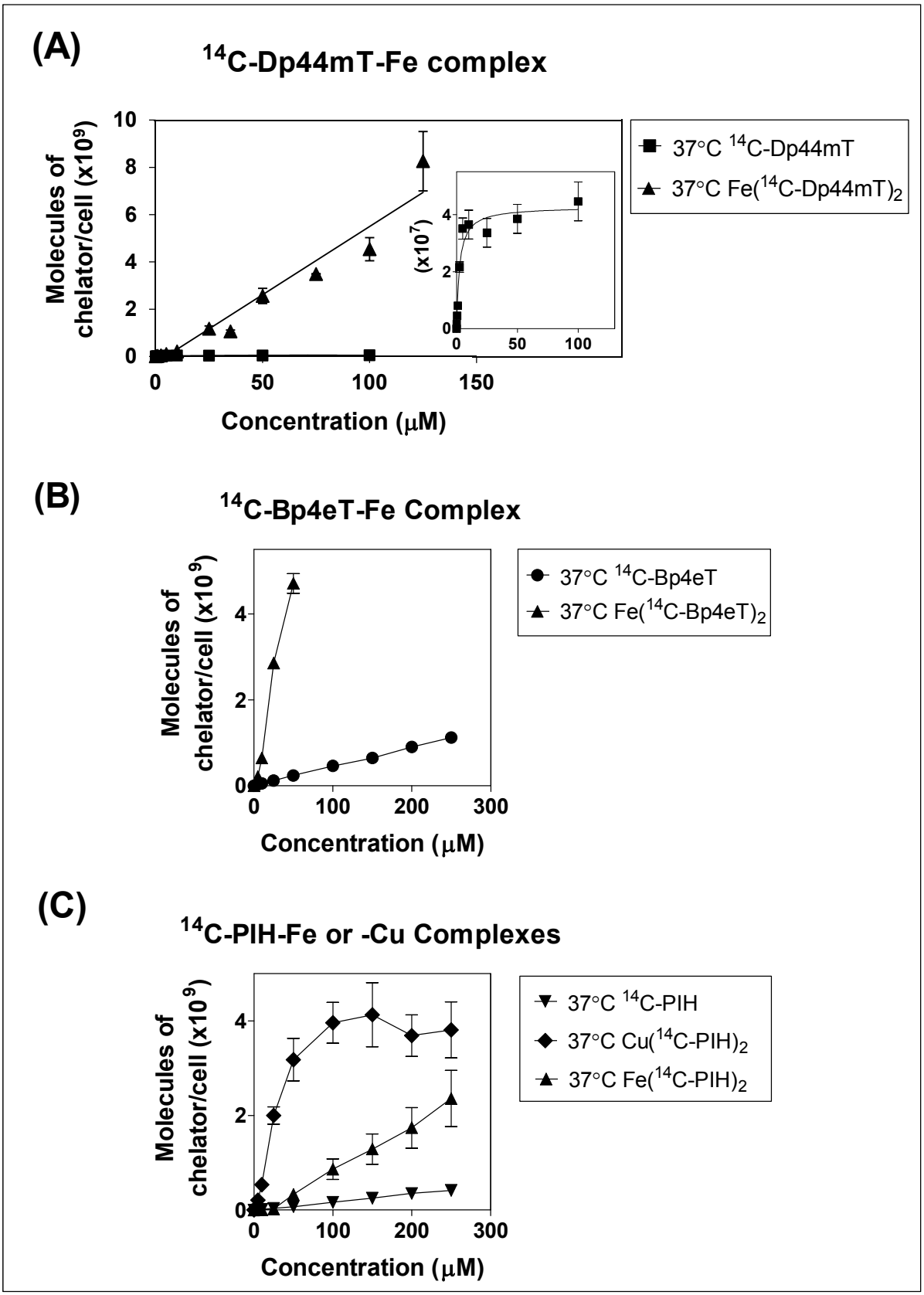

Figure 7

Molecular Pharmacology Fast Forward. Published on October 1, 2013 as DOI: 10.1124/mol.113.088393
This article has not been copyedited and formatted. The final version may differ from this version.

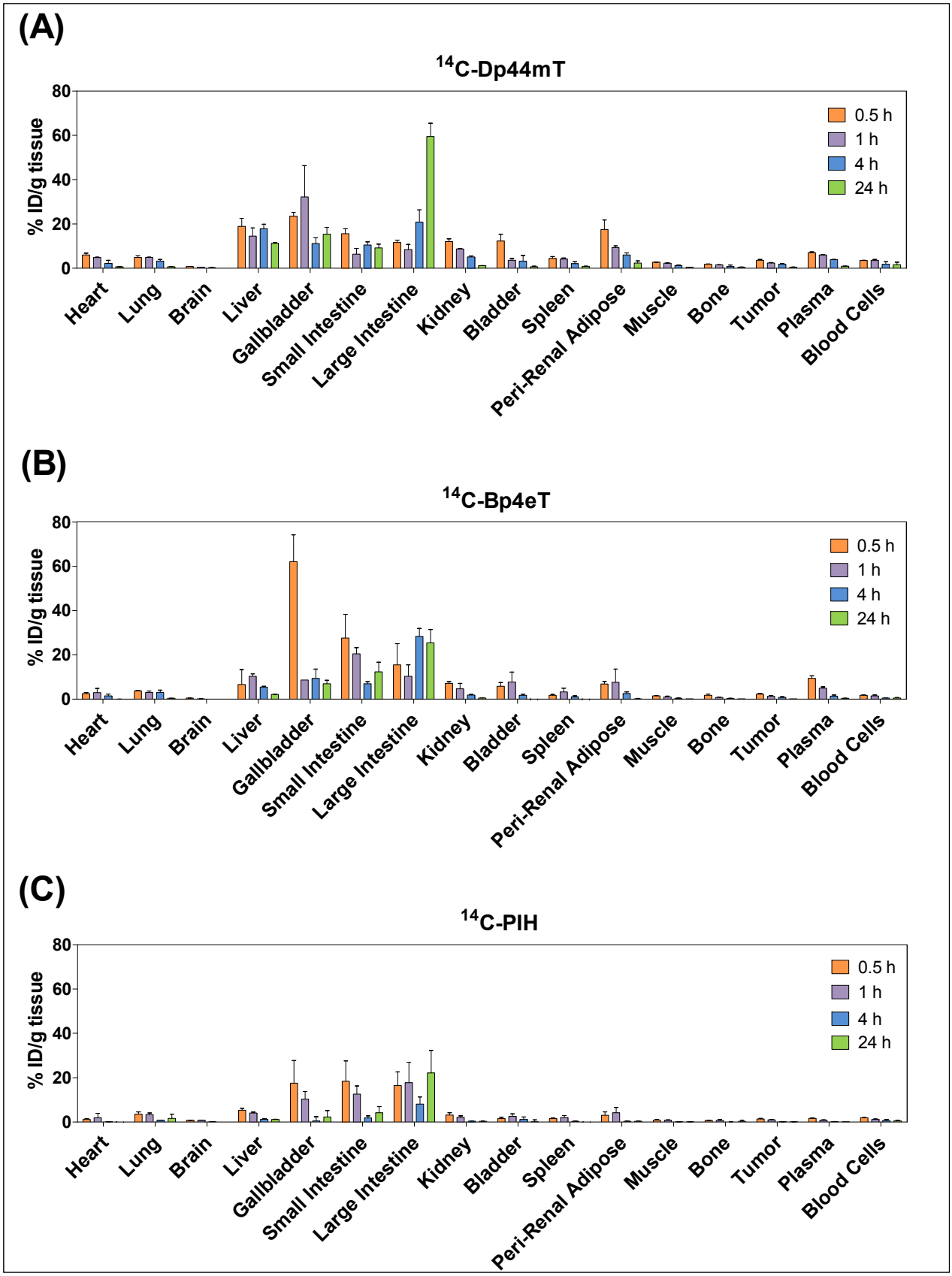

Figure 8

Molecular Pharmacology Fast Forward. Published on October 1, 2013 as DOI: 10.1124/mol.113.088393
This article has not been copyedited and formatted. The final version may differ from this version.

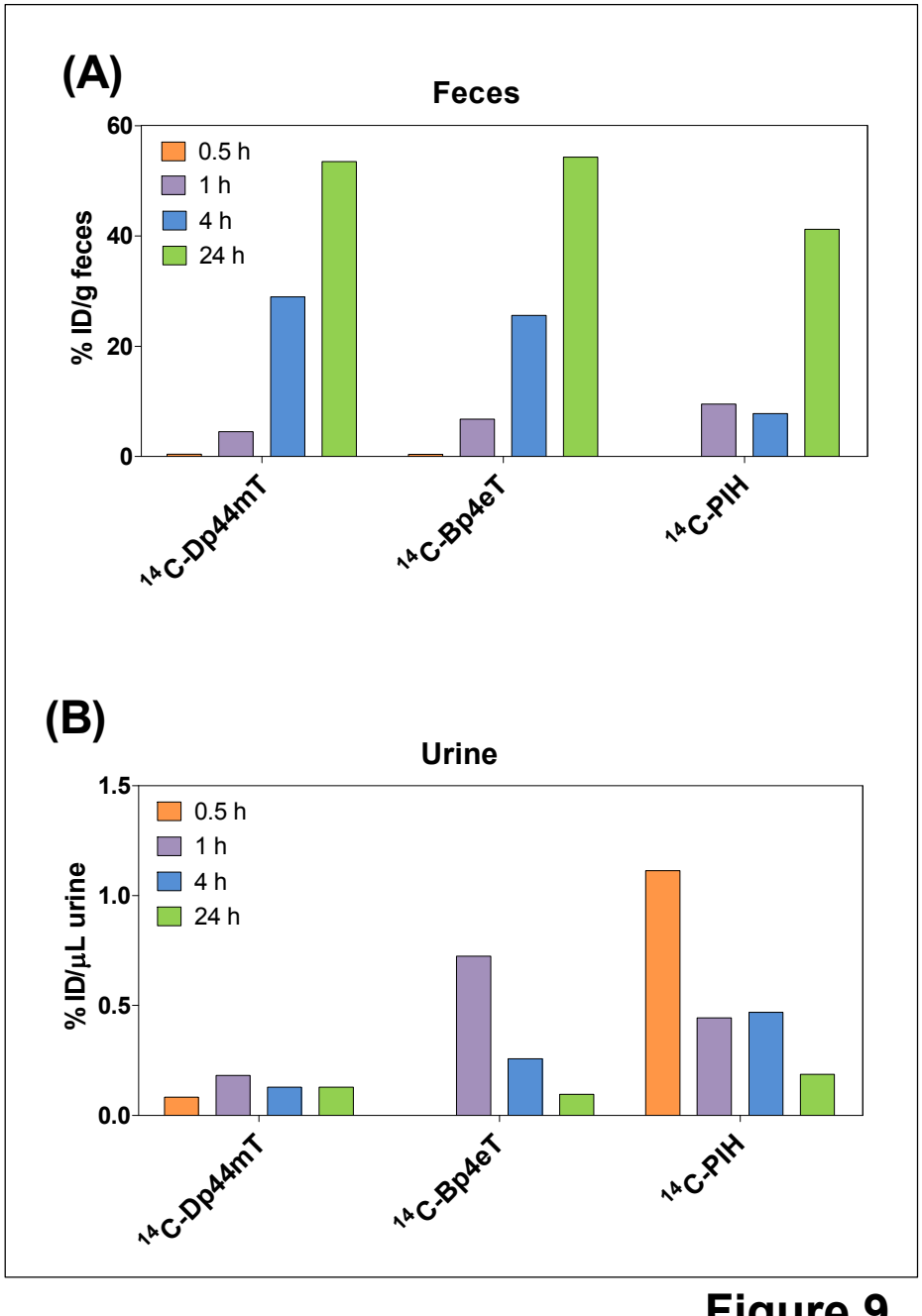

Figure 9